



ARCHIVES
of
FOUNDRY ENGINEERING

ISSN (2299-2944)
Volume 2022
Issue 2/2022

25 – 49

10.24425/afe.2022.140223

4/2



Published quarterly as the organ of the Foundry Commission of the Polish Academy of Sciences

Hot Tearing, Parameters, and Mould Types for Observation – Review

Akhyar 

Department of Mechanical Engineering, Univeritas Syiah Kuala, Jl. Syech Aburrauf No.7, Darussalam, Banda Aceh, 23111, Indonesia

Corresponding author. E-mail address: akhyar@unsyiah.ac.id

Received 20.01.2022; accepted in revised form 15.03.2022; available online 10.05.2022

Abstract

Hot tearing is a casting defect responsible for external and internal cracks on casting products. This irregular undesired formation is often observed during solidification and freezing. The solidification of molten metal also causes thermal contraction and shrinkage, indicating the occurrence of hot tearing when the alloy is restrained by the mould design. The parameters affecting this process include the pouring and mould temperatures, the chemical composition of the alloy, and the mould shape. Also, the factors affecting hot tearing susceptibility include pouring and mould temperatures, the grain refiner, as well as pouring speed. There are many methods of measuring the level of susceptibility to hot tearing, one of which is the thermal contraction evaluation during metal solidification, observed in cast products through several mould types. This paper discusses the hot tearing overview, the effect of pouring temperature, mould temperature, grain refiner, pouring speed on hot tearing, the type of mould, and criterion for hot tear observation.

Keywords: Hot tearing susceptibility, Pouring temperature, Mould temperature, Grain refiner

1. Hot Tearing

Hot tearing is a common and serious defect that often occurs during metal solidification. It is also known as hot cracking, shortness, or brittleness. Besides the name, this is a permanent defect that occurs in the form of cracks, either on the surface or within the cast product. Hot tearing is generally large and visible to the naked eye, although it is occasionally smaller in size, requiring inspection through magnetic particle equipment, radiography (x-ray), x-ray tomography, ultrasound, penetrating dyes, etc. This generally contains a major crack and many small branches, which corresponds to an intergranular path, with a surface failure view indicating a dendritic morphology. Hot tearing has reportedly been studied extensively, with many test techniques and computational models subsequently developed. Furthermore, various previous studies showed that this was a complex phenomenon, which depended on the influence of heat, fluid, and mass flows, as well as several formulation variables such as alloy composition, mould

properties, casting design, and process parameters. The grain structure refines and casting control also reduces the formation process. Over the years, several previous studies have been found to specifically study the mechanism of hot tearing formation, where shrinkage and thermal deformation during solidification reportedly caused the occurrence of metallic cracking. However, the controlling factor for this formation is still unclear [1]. With no clear standard, reliable predictive models were urgently required to measure hot tearing (or control).

The first attempt to understand the mechanism of hot tearing formation was conducted in a systematic study of carbon steel. This indicated that hot tearing was intentionally produced with flanged steel bar moulds, where the contraction of the molten metal was constrained by the rim ends of the rods [2]. The results showed that hot tearing occurred between 1,250 to 1,300°C. The evolution of stress during solidification was performed through steel bar moulds [3]. This was the continuation of the study conducted [4], where the steel bars were designed with no sharp thermal gradient. This



indicated that the cast sample did not break under the alloy contraction on solidification. Although the results did not address the actual amount of stress required for hot tearing formation, load-carrying ability under sustained contraction was still indicated. Moreover, the study of the hot tearing in aluminium alloys was caused by the stresses formed by the contraction of the main crystal during solidification [5]. In the early stages of clotting, coherent tissue was not formed and hot tearing did not occur. A coherent network is often defined when the dendrites develop and interact with one other. Based on the study, continuous freezing and stress were produced due to the growing interactions between the dendritic networks. When the molten metal shrinks, the potential solid is retained by the mould, causing the contraction of the alloy. The study subsequently explained the influential importance of the eutectic component. This indicated that when the eutectic fluid, volume, and feeding are available, sufficient, and adequate, the healing of the newly-formed hot tearing was guaranteed.

Hot tearing was formed when there was a small amount of available residual liquid, indicating that the strength of the metal increased with decreasing freezing temperature. The hypothesis stated that brittle alloy ranged between the initial dendritic formation and solidus temperatures, indicating that the metal was prone to hot tearing due to having low ductility. These early studies assumed that hot tearing was caused by the build-up of stress (combined stresses) on the metal during solidification and cooling, due to contractive restraint or obstruction. In addition, the consideration of the healing effects on the remaining available fluids is very important [6]. The initiation of hot tearing was evaluated using radiography and the thermal analysis of solidification. This introduced the concept of the liquid film during the last stage of solidification, where the formation of hot tearing began when the metallic temperature was above the solidus point (when a continuous thin liquid film was still present between the solidified dendrites). During freezing, the mechanism for this formation was the film separation (thin layer in the form of liquid metal), where the alloy approached the solidus for a few minutes and the liquid remained. At this stage, the theory of the formation of hot tearing was proposed based on the accumulation of the strain and the concept of a liquid film. This indicated that hot tearing was a strain-controlled phenomenon. The results showed that when the strain accumulated in the hot spot of the initial stage and achieved a critical value, the film was relatively thick and continuous between the dendrites [7]. In addition, the solid phase inhibiting the supply of liquid metal (feeding) was the main cause of hot tearing, which was unlikely to occur with the availability of sufficient feeding during freezing [8].

Based on interdendritic liquid films, a theory was developed [9], where surface tension was a critical factor in the formation of hot tearing, as shown in Fig. 1. This indicated that the grain structure of the metal was simplified and assumed to be rectangular. Also, the grains at positions A and B shifted in opposite directions, with the extension between them increasing as shrinkage progressed. Tearing was also likely to be formed with one of the liquid films when the movement achieved a specific value. To separate this film into two new surfaces, the stress should be greater than the molecular adhesion force, as calculated by equation (1).

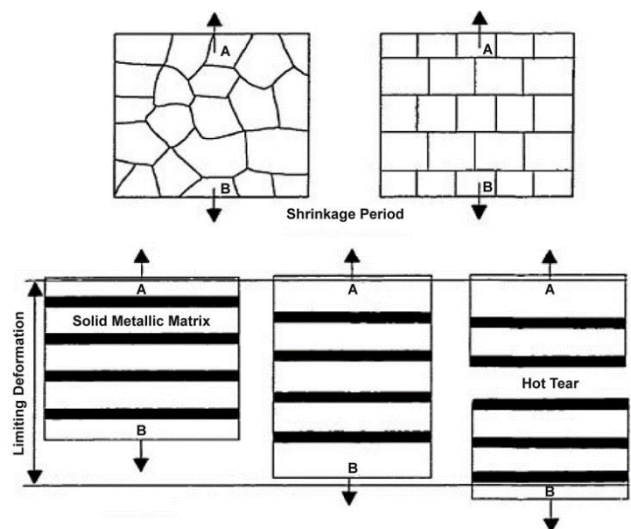


Fig. 1. The formation of hot tearing is based on the concept of liquid film interdendritic [9]

$$P = \frac{2 \alpha F}{1000 g b} \quad (1)$$

where,

P = the force required to form a hot tearing (N),

α = the surface tension of the liquid (erg/cm²),

F = the contact area between the plate and liquid (cm²),

g = the gravitational acceleration constant (cm/s²),

b = the thickness of the liquid layer between the plates (cm).

Based on the study, the theory emphasized that film thickness was considered more important than surface tension. This was due to the film thickness variation being greater than the surface tension with a change in grain size. This explanation explained the reasons fine-grained alloys were more resistant to hot tearing.

A fundamental study of hot tearing was conducted through the shear test, where the strain rate was reportedly very important for formation. Hot tearing was found to be the result of stretch accommodation, leading to the progressive separation between dendrites [10]. Moreover, a quantitative study of the freezing and crack evaluation of aluminium-magnesium alloys was carried out [11], which focused on solidification time in the mushy (metal) state. It also assumed that hot tearing was the result of uniaxial stress. This indicated that the final stage of coagulation was a very important condition for hot tearing formation, where the grains were unable to move freely. It also showed the gradual formation of the strain, which eventually caused hot tearing. Based on this theory, a hot tearing criterion with the CSC formula (crack susceptibility criterion) was developed. Hot tearing was caused by the failure of uniaxial tension in the weak part of a cast product, indicating differences with the theory based on feeding difficulties. This showed that the hydrostatic, such as triaxial, stress obtained from feeding was attributed to the formation of porosity between the dendrites [12]. In addition, an equation was developed based on Pellini's theory of strain (ϵ) in hot spots, as shown in equation (2).

$$\varepsilon = \alpha \Delta T \frac{L}{l} \quad (2)$$

where,

- \mathcal{E} = the stretch in hot spot area (%),
- α = the thermal expansion coefficient ($^{\circ}\text{C}^{-1}$),
- ΔT = the Mushy area length ($^{\circ}\text{C}$),
- L = the cast product length (mm),
- l = the long hot spot area (mm).

This equation indicated that the strain decreased with the resultant temperature difference, causing the hot spot to subsequently reduce. The hot tearing caused by the embrittlement of molten metal was examined through Griffith's crack theory. The developed model showed that the strain energy was stored in the material deformation, contributing to creating a new surface with the development of the crack. During plastic deformation, most of the fracture energy in ductile materials was applied to the root of the crack tip growth. However, the ductility was almost absent, indicating that the fracture stress is small when the metal was still molten. It also showed that the measured cleavage energy was almost the same as the surface free power. This indicated that molten metal embrittlement (hot tearing) was caused by a small level of surface-free energy between the liquid and solid phases, leading to cracks or fluid discontinuities [13]. An experiment was conducted to confirm the temperature responsible for the hot tearing formation, through a casting rig. This indicated the provision of a window above the hot spot area on the device, to observe the formation and growth of hot tearing. The load was also simultaneously measured when the metal alloy was in the mushy zone condition. Using Al-Cu alloys, this was initially produced from the formation of a very low load, with the temperature being determined between 93 and 96% of the solid material temperature [14]. Although the subject of hot tearing was not a simple discussion, the theory was still summarized into two major groups [1].

1. The first group was based on stress, strain, and SR (strain rate), due to being responsible for the thermo-mechanical properties of alloys.
2. This was based on the liquid film and feeding deficiencies related to metallurgical factors.

Based on these groups, hot tearing was reportedly a complex phenomenon combining metallurgical and thermo-mechanical interactions. Although the basic phenomena involved in this formation were quite comprehensive, there was still no agreement on the causes of hot tearing or the controlling factors [1]. This was influenced by several factors including pouring and mould temperatures.

2. Parameter of Pouring Temperature

The created different groups of opinions on the casting of steel, especially the carbon content and temperature effect, which depended on the type of product and the practice being utilized [7]. The high pouring temperature initially minimized the formation of hot tearing [15]. Meanwhile, the hot tearing was likely to occur and

be more severe at high pour temperatures. These conflicting experimental results and opinion differences were all observed in non-ferrous alloys [16]. Six binary aluminium alloy systems were evaluated, with the results showing that the fracture susceptibility reduced with decreasing casting temperature at each level of the element [6]. However, the variation in pouring temperature did not have a significant effect on hot tears [17].

The high pouring temperature was responsible for the following roles, (1) distribution of hot spots, which reduced the tendency of hot tears, and (2) increased the presence of the liquid film, leading to an increase in the tendency of hot tears [18]. However, the high pouring temperature levels increased the thermal gradient during freezing, leading to the promotion of columnar dendritic development. This indicated that columnar structure alloys had a higher casting temperature than the equiaxed types [3].

The effect of temperature differences between 750-775 $^{\circ}\text{C}$ on Al-1 wt.%Sn alloys was conducted. The results showed that both pour temperatures were insufficient to investigate the thermal effects on crack formation [19]. This indicated the differential effects of the casting temperatures, namely 675, 700, 750, and 800 $^{\circ}\text{C}$, on the susceptibility of hot tearing, during the modelling with T-Shape moulds on aluminium alloy A206. The results showed that the solid fraction was critical with increasing time as superheating increased, indicating that the alloy was more susceptible to hot tearing. Also, a correlation between the solid fraction and the pouring temperature was observed. This indicated that the critical solid fraction was obtained between 0.9 and 0.99, leading to an increase in the susceptibility to hot tearing. The model fraction occurred at a pouring temperature of 675 $^{\circ}\text{C}$, with a time of 83 s. This indicated that the higher pouring temperature of 800 $^{\circ}\text{C}$ occurred at 125 s, leading to an increase in the susceptibility to hot tearing [20].

The effect of pouring temperature (pouring, superheat, and casting) on hot cracking was reportedly studied using ring casting moulds on Al-4.5wt.%Cu and Al-7wt.%Si alloys. In the study, three temperature variations of 670, 720, and 770 $^{\circ}\text{C}$ were used for the Al-4.5 wt.%Cu alloy (superheat temperatures of 24, 74, and 124 $^{\circ}\text{C}$). Meanwhile, the temperature of 737 $^{\circ}\text{C}$ (superheat temperature of 124 $^{\circ}\text{C}$) was provided to the Al-7wt.%Si alloy. The results showed that hot tearing significantly reduced with decreasing pouring temperature [21]. Another previous study also showed that the effect of three different pouring temperatures (700, 750, and 800 $^{\circ}\text{C}$) was predicted for A356 and M206 alloys on hot tearing susceptibility. This indicated that the tendency of hot tearing slightly improved with increasing pouring temperature [22]. The effect of pour temperature on hot tearing was also studied in the NZ30K alloys with CRC moulds. The differences in the utilized pouring temperatures were 973, 1003, 1033, and 1063 K, with the superheat calcination being 60, 90, 120, and 150 K (superheat temperature = $T_{\text{pouring}} - T_{\text{liquidus}}$). Furthermore, the pouring temperatures for the AZ91D alloy were 931, 961, 991, and 1021 K. The results showed that the pouring temperature only had little effect on the bycatch at low mould temperatures (341 and 423 K for the AZ91D and NZ30K alloys). Therefore, the recommended temperatures for AZ91D and NZ30K alloys were 961-991 and 1003-1033 K, respectively [23].

Using a horizontally constrained rod casting modified (CRCM) metal mould, the effect of pouring temperature on Al-1,19wt.%Si alloy was also studied [24], where the three utilized thermal values

were 710, 760, and 810°C. The results show that hot tearing increased and subsequently decreased at pouring temperatures of 760 and 810°C, respectively. The effect of pouring temperatures (700, 750, and 780°C) on the hot tearing susceptibility of A206, A518, and A713 alloys was conducted through Ring Casting sand moulds. The results show that these temperatures had significant effects on the hot tearing and grain size of the three alloys. This indicated that pouring temperature was a critical parameter to predict crack susceptibility. Therefore, a good correlation between the pouring temperature, crack susceptibility, and grain size was observed [25]. Several studies showed that the effect of pouring temperature was the variation of the test often studied and other factors, such as cooling rate, grain shape, and metal fluidity. However, hot tearing should be considered as a product of many factors, with the measurements of crack length and formation being indirect and convoluted approaches. Besides that, linking these factors to the cause (symptoms) of formation is not very helpful. This indicates that discriminatory and quantitative tests are needed to link the cause of formation to the development of stresses in the cast product, which leads to hot tearing [26].

The effect of casting temperature on the Al-1.19wt%Si alloy was also analysed through a Horizontal CRCM (Constrain Rod Casting Modified) metal mould, where three pouring calcination at 710, 760, and 810°C were utilized. The results showed that hot tearing increased and decreased at pouring temperatures of 760 and 810°C, respectively [24].

3. Parameter of Mould Temperature

The mould temperature directly affected the cooling rate of the casting, leading to the performance being influenced by the microstructure of the cast product. Most studies on hot tearing were reportedly carried out by controlling the cooling rate and local freezing time. One method that was previously conducted was based on the control of the mould temperature [11,27], although the published literature on this topic was still very limited.

The effect of mould temperature on the role of grain refiner was conducted, with results showing that the cracks were more severe at 220°C (428 F) as compared to a mould temperature of 250°C (482 F) for similar treatment conditions [28]. Furthermore, the study of hot tearing susceptibility of some Mg cast alloys, with comparisons to several Al elements. The results showed that the occurrence of hot tearing was reduced at a mould temperature of 350°C (662 F) or higher [29]. The effect of mould temperature on Mg alloy, AZ91D series, was also conducted. These analyses were carried out at pouring and mould temperatures of 700°C (1292 F), as well as 140, 180, 220, 260, 300, 340, and 380°C (284, 356, 428, 500, 572, 644, and 716 F), respectively. The results showed that the mould temperature had a significant effect on hot tearing. This indicated that the severity of hot tearing progressively decreased with increasing mould temperature, indicating that 220°C (428 F) was a critical sculpt thermal value, which corresponded to a cooling rate of 18-20°C/s. At mould temperatures below 220°C (428 F), cracks were found to begin from the entire surface, propagate to the centre, and interconnect throughout the cross-section. However, cracks formed similar hairlines and did not connect at temperatures higher than 220°C (428 F). Based on the study, the temperatures above 340°C (644 F) were effective enough to reduce hot tearing.

This indicated that higher mould temperatures increased feeding (supply of metal fluids) in large quantities, as well as intergranular and β -phase regions (microscopic feeding). The high mould temperature also promoted uniform casting contraction, indicating that the stress concentration and the tendency for hot tearing in the cast product were decreased [17].

The effect of granular refinement and mould temperature on the hot tearing of Al alloys (series 206 and 535) in constrained rod castings (CRC) have been studied [30]. The results showed that the phenomenon was highly dependent on the mould temperature, leading to the necessity to combine grain refinement and sculpt preheating. In the study, alloys 206.0 and 535.0 were required to have mould temperatures of > 400°C (752 F) and 300°C (572 F), respectively, to prevent hot tearing. Therefore, the grinder degraded and smoothed the interdendritic structure, which subsequently increased feeding and decreased the amount of residual liquid during the last stage of freezing. This indicated that higher mould temperature reduced hot tearing due to a better feeding process, subsequently showing that sculpt calcination led to a more effective thermal gradient. During the last stage of freezing, the strain produced in the mushy zone was calculated using commercial software simulations, where a correlation was observed between solid fraction (as a function of mould temperature) and hot tearing. This indicated that the main strain occurred lower at high mould temperatures, subsequently showing that the tendency for hot tearing was decreased in the hottest sculptures due to a reduction during solidification.

The effect of mould temperature between 250-500°C (482 to 932 F) was evaluated for binary Mg-Al alloys [31]. The results showed that an increase in the mould temperature reduced the susceptibility to hot tearing. Meanwhile, a higher mould temperature caused a greater thermal onset and a longer crack propagation time. In this study, cracks occurred at all mould temperatures, although those at higher calcination were fed by the remaining liquid and subsequently repaired. This showed that higher mould temperature led to a lower cooling rate, indicating a coarser microstructure, which produced a thicker and more continuous liquid. Therefore, a higher onset temperature led to easier recharge of metallic fluids (feeding). The effect of a higher mould temperature reduced the susceptibility of hot tearing, although the literature on the influence of PT (pouring temperature) still had limited contradictory data [1].

Using Horizontal Bar mould, the effect related to three hot tearing temperatures at 140, 260, and 380°C (284, 500, and 716°F) was also analysed on AZ91D alloy, as the results showed that the thermal contraction decreased with increasing calcination. This subsequently indicated reduced susceptibility to hot tearing [32]. Based on the hot tearing of Al-2%Cu-1%Si and 206 alloys with CRC material, the effect of mould temperature was found to be 250, 300, 400, and 450°C, as shown in Fig. 2a-b. This indicated that the increase in mould temperature decreased the HTS benefit within both alloys, as the value reduced from 21 to < 5 with between 250-450°C [33].

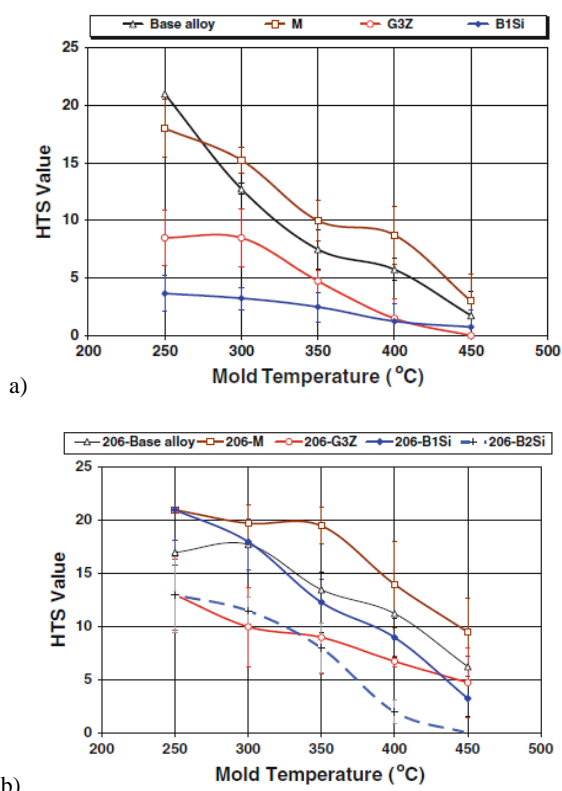


Fig. 2. (a) The HTS against the mould temperature of Al-2% Cu-1% Si with different alloys, (b) The HTS against the mould temperature for alloy 206 with different elements [33]

According to the Mg-Gd alloy hot tearing with CRC apparatus, the effect of mould temperature was 523 and 723 K (250 and 450°C). This indicated significant reductions in the total volume and susceptibility of cracks at 723 K (450°C). It also showed that high mould temperatures increased and decreased the hot spot and the total area strain [34]. Based on the hot tearing susceptibility of NZ30K and AZ91D alloys, the Temperature Different Solidus Mould (TDSM) obtained from $T_{solidus} - T_{mould}$ were 423/400, 523/300, 623/200, and 723/100 K, respectively. The mould temperatures used for the AZ91D alloy were also 341, 441, 541, and 641 K, with the results showing that this calcination significantly affected the HTS values in both metals. This indicated that the recommended mould temperatures for the AZ91D and NZ30K alloys were > 641 and 6243 K, respectively [23]. For the hot tearing of the Mg-0.2 wt% Y, Mg-1.5 wt% Y, and Mg-4 wt% Y alloys with the CRC apparatus, the effect of the mould temperature was 250 and 450°C. This indicated that the resistance of hot tearing was better at a temperature of 450°C [35]. Additionally, the effect of mould temperature was 250, 325, and 400°C on the hot tearing severity of the CRC-based B206 alloy. The result showed that the increased mould temperature significantly reduced hot tearing severity, although did not change the solid fraction [36].

4. Parameter of Grain Refiner

The effect of grain refiner with the addition of Al-5Ti-1B towards hot tearing was observed through the rig test, using variations of 0.005, 0.01, and 0.05 Ti on alloy 6061 (0.8 Si, 0.7 Mg, 0.2 Cu, 0.05 Mn, and 0.2 wt.% Cr). This showed that the grain size and Dendrite Arm Spacing (DAS) were measured using an intercept technique (according to the ASTM E112-96 standard), through the microstructure photos from a polarized light microscope. In this study, the number of solid fractions was also calculated through the ThermoCalc®, with the results showing that the addition of a grain refiner caused an equiaxed change in shape. This indicated that the alloy shrinkage caused uniform formation at the grain boundaries. When the load transfer on the surface of the granules was greater during solidification with a semisolid alloy condition (mushy zone), hot tearing is subsequently formed. This showed that the equiaxed grains in the alloy were found to be smaller, more numerous, and evenly distributed, leading to the reduction of the load transfer produced at the boundaries. Based on this condition, hot tearing was also reduced [37].

The effect of grain refiner was observed through the Al-3Ti-1B on alloys 1050, 3003, 5083, 6060, and 6082. The results showed that the addition of Al-3Ti-1B reduced the grain size, although the DAS was still relatively constant. This indicated that the grain morphology changed from being columnar (large and elongated) to cellular, without very wide dendritic tissue. In this study, the utilized mould was a CRC metal sculpture, with the results showing that bycatch was very sensitive at grain sizes above 200 µm. This indicated that the addition of a grain refiner was very effective in reducing hot tearing, due to the wider non-equilibrium freezing interval [38]. Furthermore, the effect of grain size on hot tearing, during the freezing of JIS AC7A aluminium alloy with the addition of Al-5Ti-1B and Al-5Zr on Al-25wt.%Si, in the I-beam cracking test equipment has been studied [39]. Subsequently, the study added TiB to the JIS AC7A alloy at a Ti and B ratio of 5:1, with the concentrations of Ti and B being 0.02Ti-0.004B, 0.04Ti-0.008B, and 0.08Ti-0.0016B (wt.%). The result showed that the addition of a grain refiner significantly reduced tearing susceptibility.

The effect of grain refiner with the addition of Ti-B to B206 and A319 alloys on hot tearing susceptibility was also reported through *horizontal bar casting* mould [40]. The chemical composition of the master Al-5Ti-1B alloy included Al-93.6, Ti-5.0, B-1.0, Fe-0.1, V-0.1, Si-0.06, and Zn -0.01 (wt.%), with the results showing that the addition of Ti-B to B206 and A319 alloys significantly reduced hot tearing. This was because the addition of Ti-B affected the dendrite morphology, such as the B206 structure becoming globular with the A319 remaining the same.

In the Ring Casting sand mould, the effect of grain refiner was observed with the addition of Al-5Ti-1B at 0.3, 0.7, 1.0, 1.3, 1.5, 1.7, 2.0, 2.3, 2.5, 2.8, and 3.0 (wt.pct.), on the Al-1wt.pct.Sn alloy. This indicated that the addition of a granular grinder reduced hot tearing, although did not completely prevent the condition over very long freezing ranges (Fig. 3). These results were generally not in line with several previous studies [19]. Using Horizontal Bar Casting metal moulds, Al-5Ti-1B master alloy was used as a grain refinement on B206 aluminium material. This was due to the residual strain measurement being carried out through Neutron Diffraction. The result showed that grain refinement decreased hot tearing, based on the significant reduction of the residual strain. The

homogeneity of this strain also increased with the addition of the granular refiner. Therefore, the grain refinement in casting decreased the formation of hot tearing [36].

By alloying 6,060 with Al-3Ti-1B at 0.01%Ti, 0.02%Ti, and 0.05%Ti, a granular refinement study was observed, indicating that the process affected hot tearing due to the changes in grain morphology. This showed that the alloys without granular refiners were equiaxed or largely columnar. Despite the reduction of sizes through the increasing addition of finer grain, the Dendrite Arm Spacing (DAS) was still relatively constant [37]. Furthermore, the effect of grain refinement on the modified Al-Cu 206 alloy (M206) aims to prevent the composition of Ti. Using commercially pure Al, Al-50%Cu, Al-25%Mg, and Al-50%Mn master alloys, these metals are created to significantly reduce the composition of Ti, B, and other grain refiners. In the granular refinement process, the additions of the Al-Ti and Al-TiB master alloys were performed, with the grains subsequently obtained from columnar to equiaxed dendrites, as well as the globular structure. The analytical results also indicated that the grain size and morphology significantly affected the tendencies of hot tearing [1].

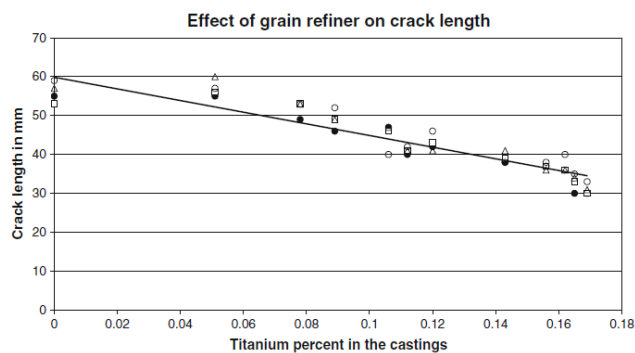


Fig. 3. The effect of grain refiner on crack length [19]

Based on the grain refinement and hot tearing susceptibility of H-13 “dog-bone shape” steel moulds, the effect of adding Al-Ti-B (Al-5Ti-1B and Al-1Ti-3B) to AZ91E alloys was also observed. This was carried out with the compositional variations in the addition of Ti, at 0.1, 0.2, 0.5, and 1.0 wt.pct. Without the addition of Ti, the results showed severe hot tearing conditions. Meanwhile, the additions of Al-5Ti-1B and Al-1Ti-3B ordinarily and significantly reduced hot tears, respectively. Moreover, the addition of Al-1Ti-3B significantly decreased the sample grain size from 113-72 μm (addition of 1.0 wt.pct.), although did not reduce the hot tear conditions. This was due to the large TiAl_3 particles increasing the stress during freezing [38]. For the Ti of 0.006 wt.pct. and A356 alloy with 0.14 Ti-value against hot tearing, a Ti grain-refining effect was observed on the M206 alloy [1]. This showed that the effects of the Al-5Ti-1B master alloy on the A206 (0.2, 0.4, and 3 wt.pct) and M206 (0.4 and 3 wt.pct) metals were carried out using a CRC mould, based on the grain refiner. The results showed that the refinement of the A206 alloy significantly reduced HTS through Ti and B [39].

The grain smoothing effect of Zr-Ti-B on Al-2% Cu-1% Si and 206 alloys also reduced hot tearing susceptibility, increased the intergranular liquid film per unit volume, and delayed the achievement of the coherence point [33]. On pure Mg alloys, the addition of the Al-5Ti-1B grain refiner was subsequently conducted

at 0.05 wt.pct, indicating that the granular agents reduced hot tearing by delaying coherence. It was also found to increase the capillary strength of the previously blended intergranular network [40]. Using the Al-5Ti-1B master alloy (93.64Al, 5.0Ti, B1.0, Fe0.1, V0.1, Si0.06, and Zn0.01 wt.pct) with B206 (0.02 and 0.05 wt.pct), the effects of Titanium (Ti) grain refiner were observed by the neutron diffraction in the CRC steel moulds. This effectively eliminated hot tears by significantly reducing and transforming the grain size and structure, respectively. It also transformed the grain structure from coarse dendrites to finer and more globular grains [36].

5. Parameter of Pouring Speed

The effect of speed on structure formation and hot tearing was carried out on Al-Cu billets during the solidification of DC casting. This indicated that the speed and billet length was measured using a displacement sensor [41]. The analysis of hot tearing on casting speed and copper (Cu) composition is shown in Fig. 4.

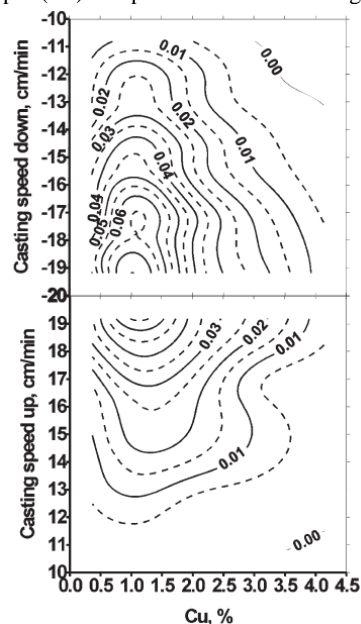


Fig. 4. The effect of casting speed and Cu concentration on the hot cracking (HCS) of Al-Cu alloys [41]

6. Measurement of Hot Tearing Susceptibility Level

The hot tearing susceptibility level was calculated using the HTS (Hot Tearing Susceptibility) formula, as shown in equation (3). This formula was obtained by assigning a value to the cracks in the cast product with several parameters, namely *NOT* (Number of Tears), *WF* (Weighing Factor), and *NOF* (Number of Casting).

$$\sum HTS = \frac{(NOT * WF)}{NOF} \quad (3)$$

where,

- HTS = The susceptibility to hot tearing defects,
- NOT = The number of hot tearing from sample repetitions for each parameter,
- WF = The hot tearing type with a provided value as shown in Fig. 5 and Table 1.
- NOF = The number of samples for each parameter.



Fig. 5. The WF for various tearing types [42]

Table 1. Assigning the value of tearing type to the cast sample [42]

No.	Tearing Types	WF Value
1	No tear	0
2	Hairline	0,25
3	Modest tearing	0,50
4	Severe tear	0,75
5	Fully broken	1

The hot tearing susceptibility category of the bycatch value was determined as follows [21,42]:

- < 0.5 = no hot tearing susceptibility,
- 0,5 – 1.25 = small tearing susceptibility,
- 1.25 – 2.25 = moderate tearing susceptibility,
- 2.25 – 3.5 = high hot tearing susceptibility,
- > 3.5 = very high hot tearing susceptibility.

The HTS calculations for CRCM-H that have been modified from CRC to assess the severity of more complex tears. Using equation (4), Fig. 6, and Fig. 7, the HTS parameter was used to evaluate the hot tearing susceptibility.

$$HTS = \sum C_i \cdot L_i \cdot P_i \quad (4)$$

where, HTS = the total hot tearing susceptibility of the metal alloy casting, C_i = the numerical value used to represent the hot tearing susceptibility level in the rod, L_i = the length rating of each hot tearing, and P_i = the tearing position (Table 2).

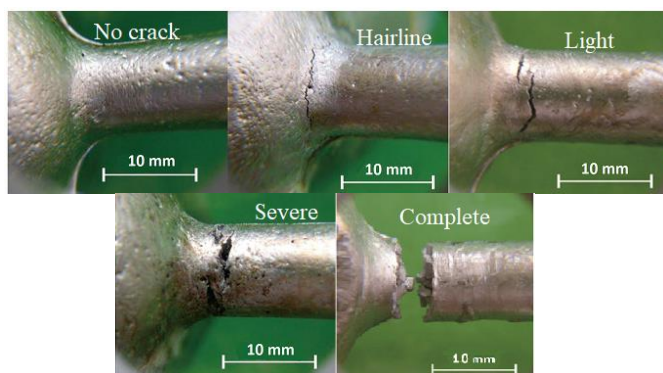


Fig. 6. Typical hot-tearing on the casting surface [43]

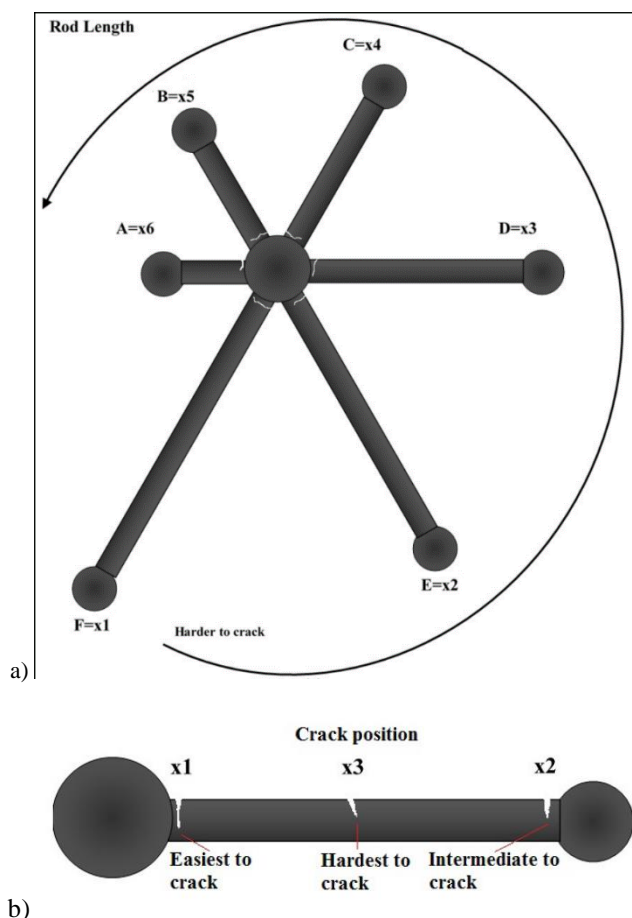


Fig. 7. Determine of HTS number on CRCM-H based on: (a) the length of the rod and (b) the position of the crack [43].

7. Mould Type for Hot Tearing Observation

Ring Casting Mould. Fig. 8 shows a test scheme using a visual method through a ring mould [44]. This mould contained a thick steel plate with an open cavity as a ring source to be filled with

molten metal, while the centre was provided with a solid core. The molten metal was subsequently filled to the brim at approximately 3/4 inch high. The results showed that tensile stress occurred around the outer surface of the cast product, leading to the hot tearing of the specimen. Also, the opened surface helped to visually observe the entire freezing process.

Using an Acoustic Emission (AE) system and a thermocouple in a Ring Casting metal mould, an analysis was conducted on hot tearing [45]. This was carried out by comparing the AE signal and thermocouple cooling curves. In Fig. 8a, *in situ* experimental setups were observed through the AE system and thermocouples, with MITRAS 2001 used to translate and record acoustic sample signals. This was carried out during the solidification of molten metal, through AE probes, piezoelectric transducers, and pre-amplifiers. A 10 cm long AE probe and K-type thermocouple were also used to record the acoustic signal and casting heat, respectively, with the utilized material being the AA1050 alloy.

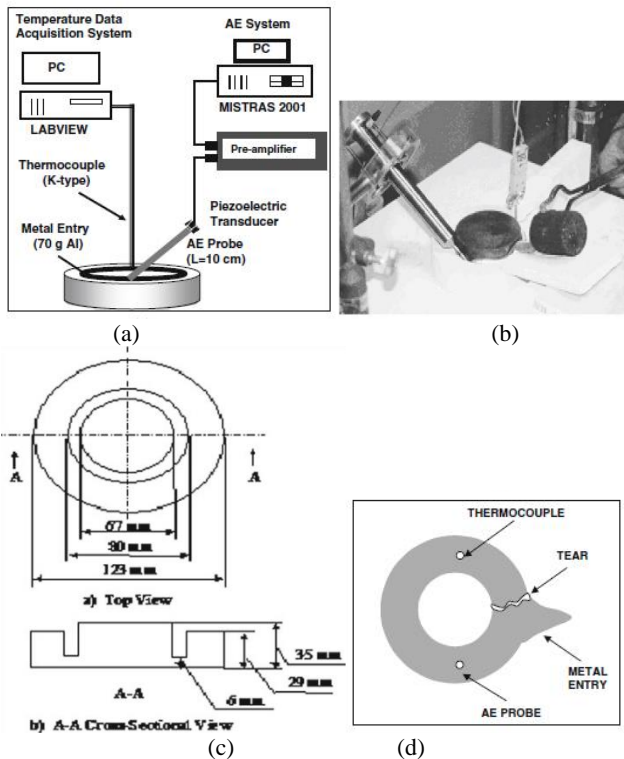


Fig. 8. (a) The experimental AE scheme, (b) The experimental setup casting, (c) The Ring-Casting scheme, and (d) The probe-thermocouple AE position [45]

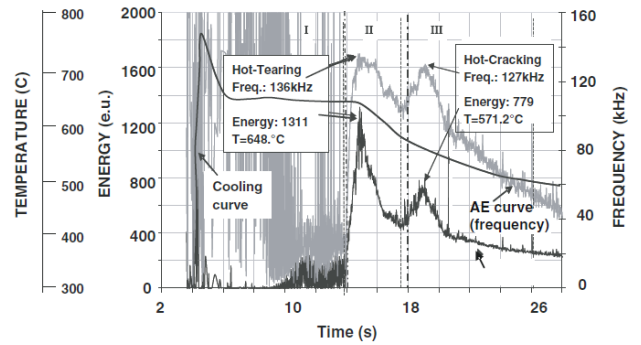


Fig. 9. The graph of the temperature (°C) and average frequency of AE (kHz) towards the solidification period (s) of the metal [45]

Hot tearing and cracking were determined by combining (superimposing) the AE signal and the cooling curves, which were subsequently divided into three zones (Fig. 9). Zone I showed the frequency curve and the amplitude distribution, subsequently indicating the absence of the aluminium solidification properties. Meanwhile, the presence of interdendritic friction and thermal shock was observed in this zone [45]. According to Purvis, the turbulence of the molten alloy disguised the freezing of aluminium at the beginning of casting, based on the slight quickness of the solidification process in the ring metal moulds [46,47]. This theoretically states that hot tearing is a macroscopic occurrence at the temperatures above the solidus when the metal is in a semi-solid state. However, hot cracking occurs below the solidus temperature when the molten metal is completely solid. Fig. 9 shows that the peaks of zones II and III acoustic signals occur at the conditions before the solidus, subsequently indicating the actions of hot tearing and cracking [45].

Based on Al-1 wt% Sn materials, hot tearing was analysed through the ring casting on four concurrently aligned ring-shaped samples [19,48]. Fig. 10 a and b show the dimensions of a single ring casting pattern, as well as the inlet sequence and four steel cores within the mould, respectively. This indicated that the mould contained sodium silicate sand with CO₂ reinforcement. In this condition, the molten metal was passed through a sprue in the middle of the mould, where a radial contraction was performed during solidification. This contraction was caused by the core, with cracks subsequently formed in the specimen. In addition, hot tearing was calculated from the average cracks of the four rings.

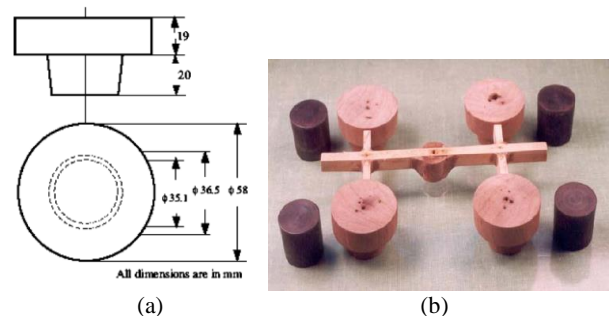


Fig. 10. (a) The single ring casting pattern scheme, and (b) The inlet wood pattern with four steel cores [19]

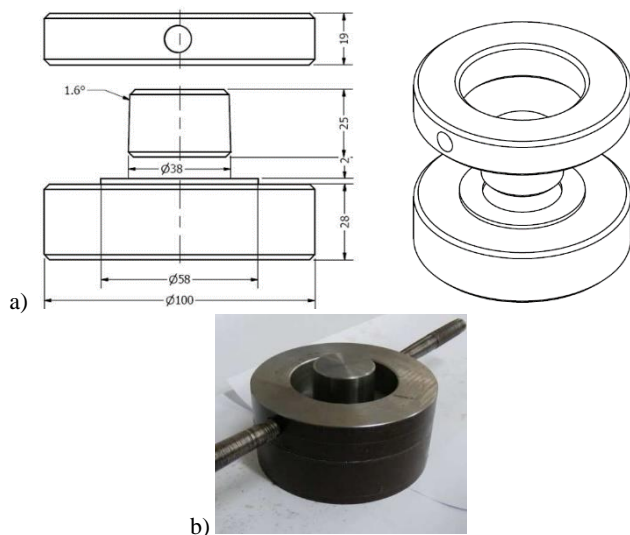


Fig. 11. The ring casting mould (a) ring mould scheme, and (b) photography ring mould [21]

Hot cracking was analysed using a ring casting steel mould, as shown in Fig. 11. This mould was ring-shaped with inner, outer, and core diameters of 58, 100, and 38 mm, as well as a height of 19 mm, respectively.

The samples were directly observed and analysed, with hot crack being assessed using Eq. (5) and the HCI (Hot Cracking Index).

$$HCI = \frac{\sum(NOC \times WF)}{NOF} \quad (5)$$

where NOC = the number of cracks, WF = the weighting factor based on the level of hot cracking (namely, not cracked WF=0, hairline crack WF=0.25, modes crack WF=0.5, severe crack WF=0.75, and complete crack WF= 1), and NOF = the number of casting. Furthermore, HIC follows:

- < 0.5 no hot cracking susceptibility
- 0.5 – 1.25 small hot cracking susceptibility
- 1.25 – 2.25 moderate hot cracking susceptibility
- 2.25 – 3.5 high hot cracking susceptibility
- > 3.5 very high hot cracking susceptibility

Flanged Bar Mould, Fig. 12 shows a schematic of the flanged bar casting mould used [49], whose study was developed from the pure hot tearing theory, which involved the linkage of stress and strain in the visual method of RCM (ring casting moulds). In this study, a sand mould as a flanged bar was used, where the hot spot area was conditioned at a constant cross-sectional area along the rod. During solidification, the contraction of the metal alloy occurred along the rod, indicating that the flange resisted the metal movement due to shrinkage when frozen.

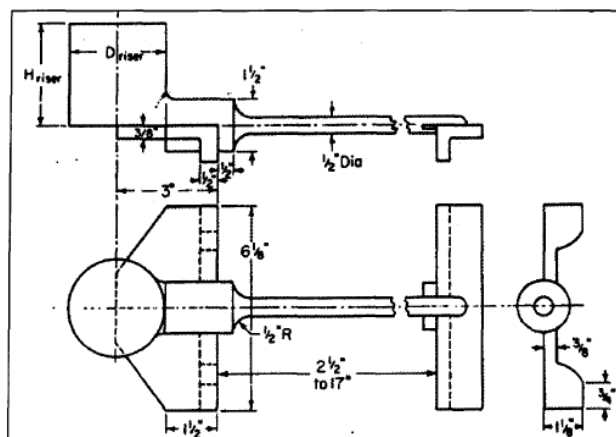


Fig. 12. The flanged bar casting mould design [49]

“U” Casting Mould, Based on Fig. 13, a visual test method with a “U” casting mould was observed, to determine the hot tearing resistance of aluminium and magnesium alloys [39]. This mould was used to observe the hot tearing susceptibility and the effect of the sensitivity level. The cross-section of the specimen was rectangular with a thickness and width of 3/4 and 3/8 inches, respectively. The stem length also varied between 2-8 inches, with a fillet radius ranging from 3/4 inch to a sharp angle. In addition, the measured hot tearing value was compared with the sharpness of the angle and fillet radius on the mould.

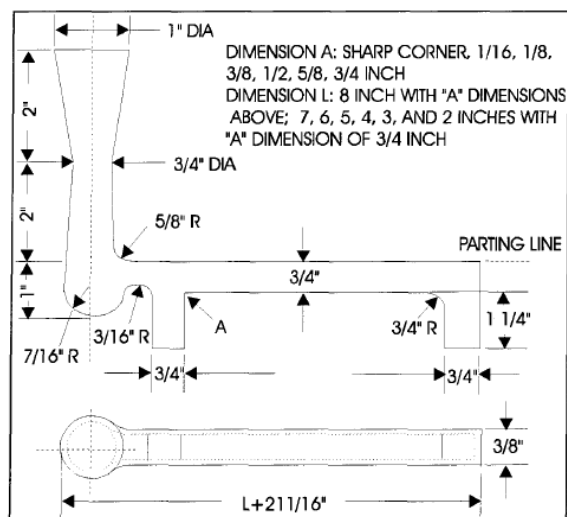


Fig. 13. The “U” casting mould [50]

U-Shaped Casting, A hot tearing analysis using a U-Shape mould was also carried out [51] as shown in Fig. 14, with the calculation formula presented in Table 3.

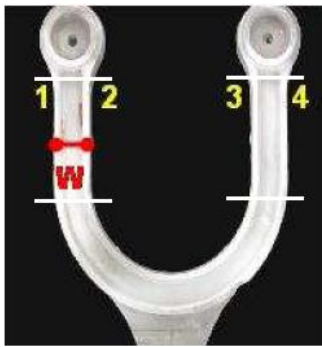


Fig. 14. The U-Shape Casting [51]

Table 3.
The calculation of hot tearing susceptibility index [51]

$HTS\ index = \sum N_{tear\ rating}$			
None	Spot tears	$\leq W$	$> W$
W" shows the width of the arm			

Ball-bar mould, According to Fig. 15, a visual test method was utilized for hot tearing, through a ball-bar casting mould [18], which is spherical at the base of the continuous long thin cylindrical rods. Also, a flange was created at the end of the mould as a retainer, with varying lengths and diameters. The tearing produced on the shortest stem was then used as a parameter for measuring hot shortness. For each alloy test, the hot tearing tendency was related to the maximum length of the casting mould, with results showing that a longer stem led to more susceptibility.

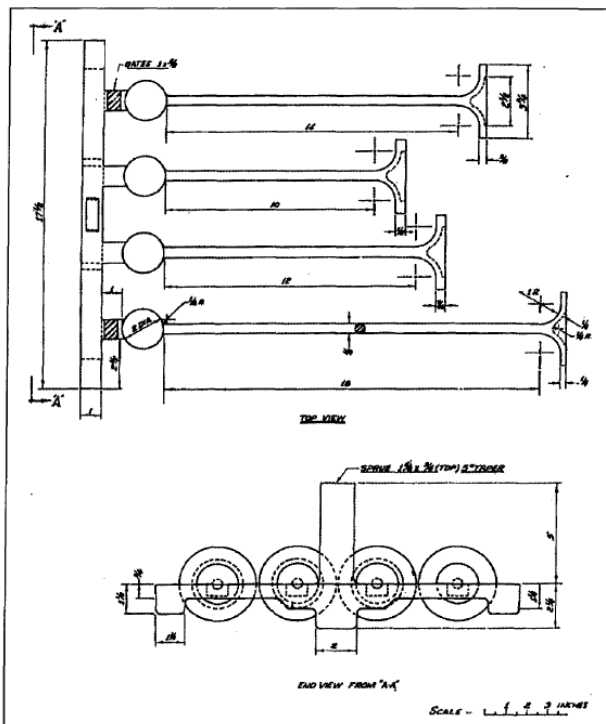


Fig. 15. The ball-bar casting mould [18]

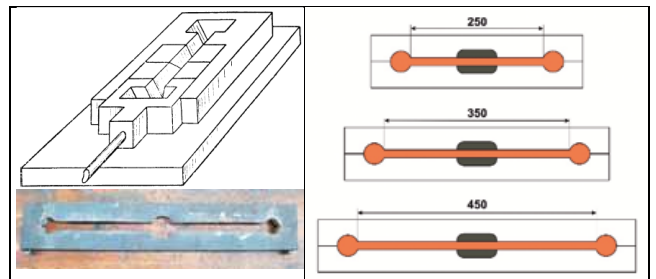


Fig. 16. The hot tearing test with dog-bone mould [52, 53]

Dog-bone Mould, Fig. 16 shows the hot tearing test method with a backbone-shaped mould [52], where the configuration and dimensions varied by sliding the end of the sculpt. In this study, the molten metal was filled in the middle of the mould, which was constrained at both edges. During freezing, the stress was concentrated in the centre of the specimen, which started from the edges (walls) of the mould. The tearing formed during this stage was measured to determine susceptibility.

Tatura star test (harp test), Fig. 17 presents the modification of the previous backbone mould, where six-rod lengths were used to measure the hot tearing susceptibility [40]. This indicated that the hot cracking sensitivity indexes were obtained from the minimum critical length (L_{cr}) for the six-length variations observed in the specimen, whose diameter varied between 4-16 mm. Meanwhile, the hot tearing susceptibility indexes were obtained from the maximum critical diameter (D_{cr}).

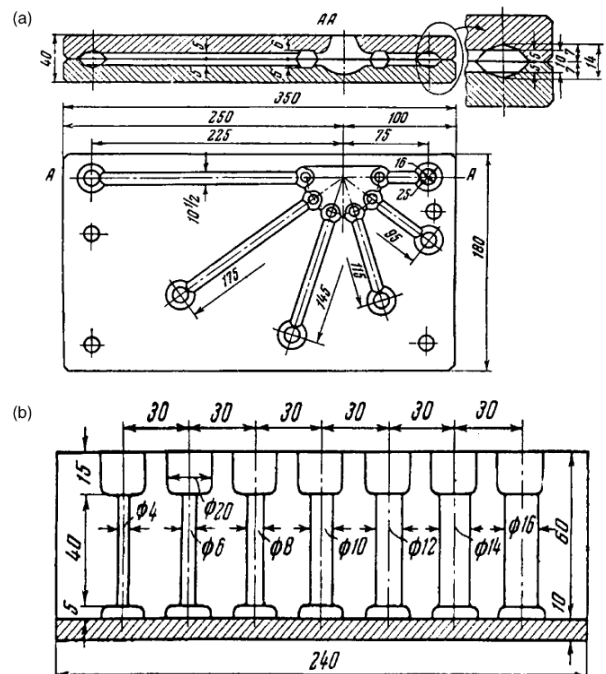


Fig. 17. The multiple dog-bones combination moulds to observe hot tearing susceptibility with (a) variations in stem length, and (b) variations in diameter [52]

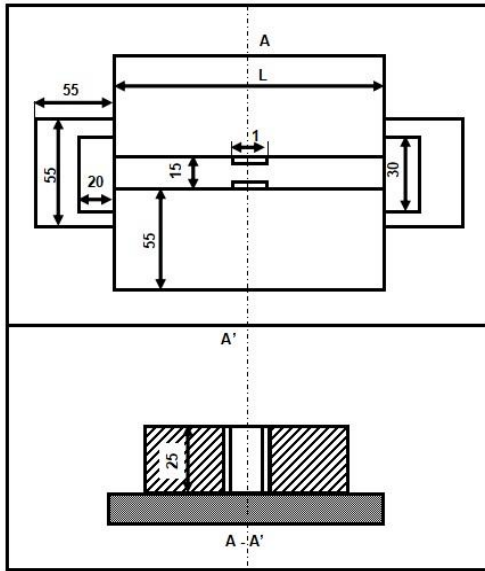


Fig. 18. The I-beam casting [54]

Based on Fig. 18, a schematic of the visual testing method was observed with the I-Beam casting moulds [54]. This mould contained a thick plate with an open cavity forming an I-shaped rod. The results showed that hot tearing occurred at the weakest area along the rod.

Chilled Casting Mould. According to Fig. 19, a visual test method was described with chilled casting moulds, designed to approximate DC casting simulations [55]. Study conditions such as the thickness of the cast product were controlled through the depth stop cooling technique. With the top of the pipe entering and exiting the cooling water, the induction furnace was used to melt the metal alloys. Furthermore, the cooling rate was similar to the shell zone of a DC aluminium ingot. This analysis was conducted to analyse the hot tearing problem occurring in the conical cylindrical steel surface area.

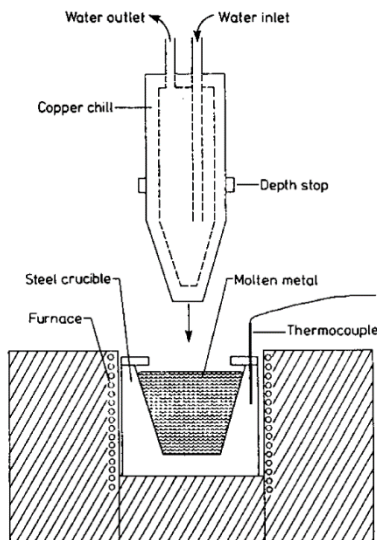


Fig. 19. The chilled casting moulds [55]

Mould Constrained Rod Casting (CRC), Fig. 20 shows a schematic of a CRC mould with four variations of cylindrical rod length, which are bounded at each end by a round cross-section. This indicated that the molten metal was filled from above through the sprue, thereby resulting in a vertical mould position. Hot tearing was quantitatively measured and formed along the cylindrical rod. This showed that the variations in the rod length affected the hot tearing formation [56].

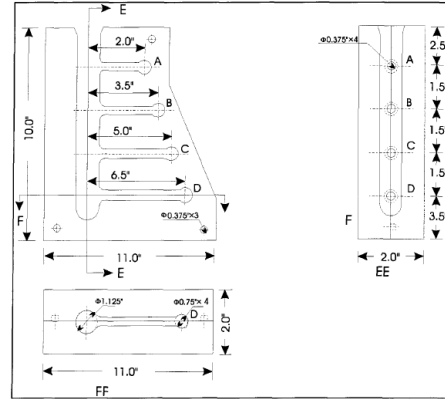
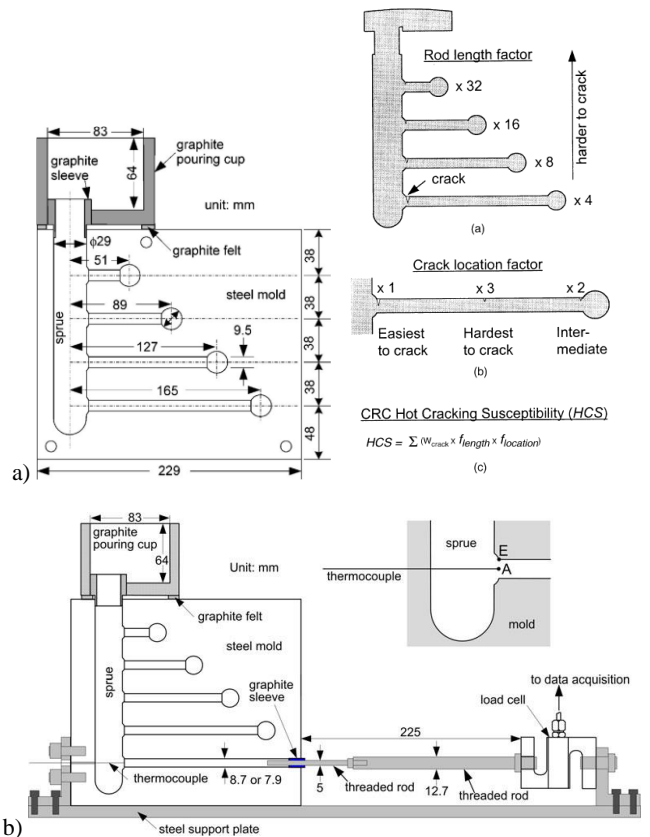


Fig. 20. The CRC mould schematic [56].



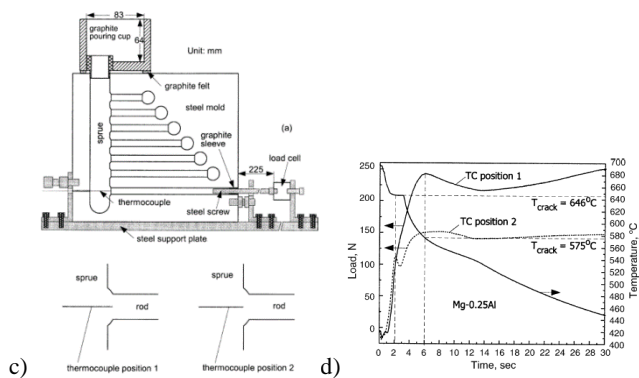


Fig. 21. (a) The Schematic of CRC mould and the measurement of hot tear value, (b) The CRC mould with loadcell, (c) The CRC mould with loadcell and increasing rod numbers, and (e) The load and cooling curves [57,67]

Hot tearing was analysed using CRC (Constrained Rod Casting) permanent moulds in metal casting and solidification [57,58,59,60,61]. The CRC was also developed on sand moulds [58], with the schematic shown in Fig. 21, where the length of the rods varied from the shortest to the longest at 51, 89, 127, and 165 mm, respectively (Fig. 21a). The diameter of all rods was also similar (9.5 mm), with each spherical cast cavity of 19 mm being provided at the end of the materials. When the molten metal solidified in the mould, the ball subsequently created a constraint, between the ball and the sprue, indicating that the rod was subjected to tensile stress due to thermal contraction. Based on Fig. 21b, an extension of the CRC template is observed for quantitative measurements, through the addition of a load cell-measuring device to the last rod [57]. This helped to determine the value of the load occurring in the metal liquid during freezing. Fig. 21c also shows the modified CRC mould, as the number of rods increased to seven. This showed that six and one rods were each observed with and without a ball, indicating that the liquid metal easily moved when shrinking. The lengths of the six rods were also observed at 70, 89, 108, 127, 146, and 165 mm respectively, with the last material added to a thermocouple to observe the cooling curve. Additionally, Fig. 21d shows the calculations of the hot tearing and cracking susceptibility values, through the length of the rod (the longest rods are more susceptible to hot tearing). Fig. 21e also shows the loadcell measurement curve, compared to the cooling result of the thermocouple.

For measuring the value of hot tearing, four formulas are shown in Eqs. (6-9), with a calculation system presented in Tables 4 and 5.

$$HCS = \sum f_{crack} f_{length} f_{location} \quad (6)$$

$$HCS = \sum W_{crack} f_{length} f_{location} \quad (7)$$

$$HTS = \sum [(L_i) \times (C_i)] \quad (8)$$

$$HTS = \frac{\sum_{i=A}^D C_i / L_i}{\sum_{i=A}^D 4 / L_i} \quad (9)$$

where HCS = Hot Cracking Susceptibility, HTS = Hot Tearing Susceptibility, f_{crack} = the crack factor, f_{length} = the length of the rod,

$f_{location}$ = the location factor for cracks in the stem, W_{crack} = the maximum crack width (mm), L_i = the length of the rod, C_i = the value of the crack type, and i = bar A, B, C, or D.

Table 4.
HCS rating system [57]

	f_{crack}	f_{length}	$F_{location}$	W_{crack}
Short hair line	1	165 mm	4 Easiest to crack (sprue end)	1 the maximum crack width measured in mm
Full hair line	2	127 mm	8 Intermediate (ball end)	2
Crack	3	89 mm	1	3
		6 mm	6	
Half broke	4	51 mm	3 Hard to crack (middle of rod)	3
		2 mm	2	
n				

Tabel 5.
HTS rating system [56]

Bar Rating	Length	L_i	Hot-Tear Rating	Severity	C_i	*If no hot tear is present, the rating is zero.
Bar Length (cm)		Hot-Tear Type*				
1	16.5	1	Hair line		1	
2	12.7	2	Light		2	
3	8.9	3	Severe		3	
4	5.1	4	complete separation		4	

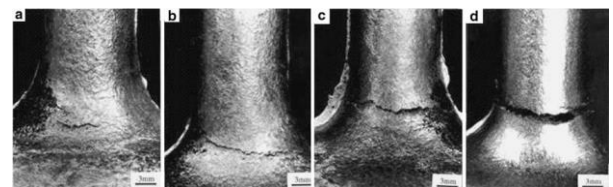


Fig. 22. The types of hot tearing defects with different levels (a) hairline, (b) light, (c) severe, and (d) complete separation [56]

Horizontal Bar Casting. Fig. 23 shows a schematic of a horizontal rod test, using a permanent steel mould. This indicated that the long horizontal rods were connected by vertical sprues and flanges at their respective ends [32]. During freezing, thermal contraction occurred along the horizontal rod due to the retention of molten metal by the sprues and flanges, leading to hot tearing. In this study, the alloy used was magnesium (AZ91D), as hot tearing susceptibility was measured using the HSI (hot tearing susceptibility index) formula in equation (10).

$$HSI = Crack Length [mm] * f_{crack} * f_{location} \quad (10)$$

where,

f_{crack} = factors that indicate the severity of hot tearing

$f_{crack} = 1$ for hair crack,

$f_{crack} = 2$ for full crack,

$f_{crack} = 3$ to crack to break on the sample,

$f_{location}$ = factors that indicate the location of the difficulty level of crack formation in the sample,

$f_{location} = 1$ for cracks occurring close to the downsprue,

$f_{location} = 2$ for cracks occurring close to the ends of the restraint rods,

$f_{location} = 3$ for cracks occurring in the centre of the rod within the sample.

Based on horizontal bars, hot tearing was investigated using the permanent moulds containing premium H-13 tool steel [32,17,36,62,63]. The length of the horizontal rod began with a specimen thickness of 20 mm from the bottom sprue (260 mm), as restraint was observed at the end of the material. Subsequently, freezing began from the end of the horizontal rod towards the pouring cup, with solidification showing a temperature gradient between the downsprue and the material. This led to the stress or deformation of the cast specimen, due to the axial contraction of the horizontal rod exceeding the semisolid strength or ductility of the alloy. Therefore, a hot tear was produced in the vicinity of the downsprue.

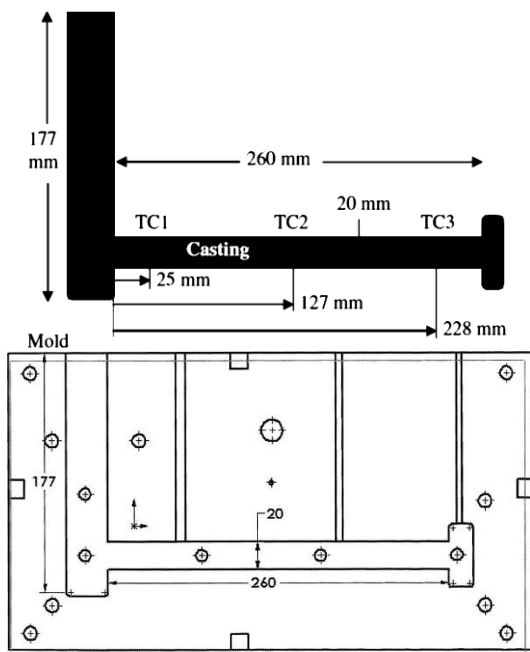


Fig. 23. The horizontal rod mould [17,32]

N-tech mould. Based on Fig. 24, an N-tech mould for hot tearing analysis is observed from the modified dog-bone testing sculpt. This indicated that five length variations of the rod and the ball served as a constraint [65]. With the heating plate placed under the mould, the sculpt temperature was controlled. The results showed hot tearing along the rods, as the longest had the highest susceptibility. In this study, the measurements contained two forms, namely qualitative and quantitative analyses, where the hot tearing index was obtained by adding the cracks to all the "dog bones". The characteristics of this phenomenon were also obtained by plotting all visible cracks [65].



Fig. 24. The N-tech mould [65]

The Test Developed in the Austrian Foundry Research Institute. Based on the test developed in the Austrian Foundry Research Institute, three methods were observed for predicting hot tears, namely TFR (Terminal Freezing Range), CSC (Creating Susceptibility Coefficient), and HCI (Hot Cracking Indexing). Firstly, the TFR method was carried out with software calculations, to simulate material solidification. Secondly, the CSC calculation was performed to correlate hot tear/crack tendency with alloy composition. Thirdly, the calculation of HCI was conducted by providing an index to the material against hot tearing. Fig. 25 shows a model used with a combination of several "dog-bone" rod lengths, which were applied to both metal and sand castings [42].



Fig. 25. The HCI method sample model [42]

The Test Developed in the Laboratory of Foundry Moulds Technology of the Faculty of Foundry Engineering. According to the Laboratory of Foundry Moulds Technology (Faculty of Foundry Engineering), continuous stress measurements were carried out during the solidification of the sand mould, which was used to determine the cooling and inhibited shrinkage rates in the casting product (Fig. 26). This subsequently affected the tendency of casting cracking, as hot tears occurred in the change line due to the geometric shape being sharply curved. The method was also used to obtain answers on the stresses produced when shrinkage was sustained, leading to the occurrence of a product defect or failure [66].

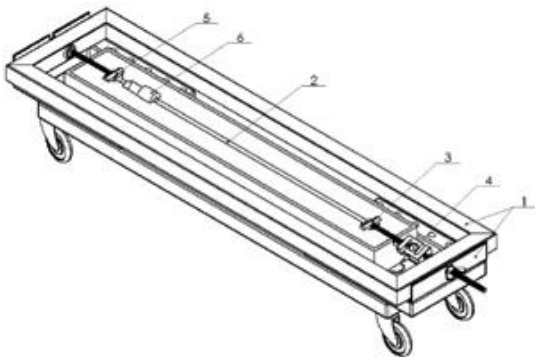
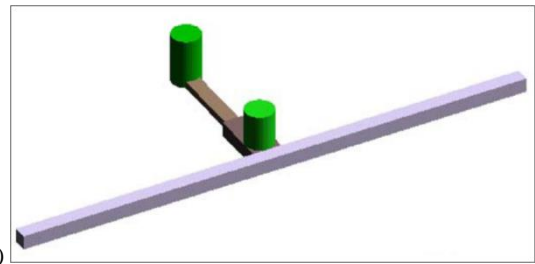
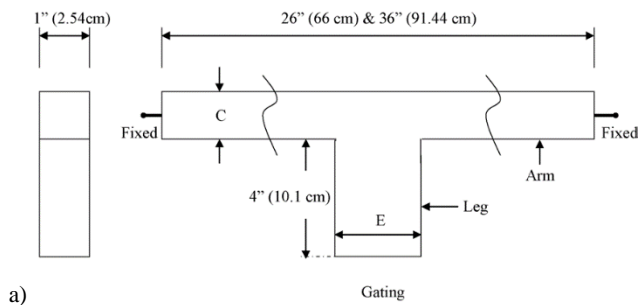


Fig. 26. The test scheme of hot tear tendency, (1) frame, (2) rod sample-sand mould, (3) fixing of the rod end, (4) tensometric system of force measuring, (5) fixing of the rod stable end, and (6) Thermo insulating insert [66]

“T” Shape Mould Casting. Several studies were conducted on hot tearing through the “T” shape casting moulds on steel materials [67,68]. A riser was added to the inlet, as variations were also observed in the sample entrance width (E), as well as the length and width (C) of the arm. Fig. 27a and 27b show the schematic “T” shape casting and the riser addition at the top of the inlet, respectively. Table 6 also shows the size variations for each arm length, C, and E, within the specimens. Meanwhile, the thickness used for the entire sample was 1.0” (2.54 cm). In this process, the bolt was placed in the cast cavity to provide zero displacements at both ends of the arm, subsequently indicating the concentration of the strain at the centre. A hot spot then occurred in the middle because the area experienced the highest strain with the material solidification. It was also due to the lack of a residual metallic fluid supply, leading to the occurrence of hot tears at that location.



b) Fig. 27. (a) The schematic of “T” shape casting and (b) The addition of a riser in the centre of the specimen arm [68]

Table 6.

The variation of “T” shape casting [67]

	Arm length	Arm width, ‘C’	Leg width, ‘E’
Without riser	26” (66 cm) - 36” (91.4 cm)	0.5”(1.27 cm) - 1.0”(2.54 cm)	1.0” (2.54 cm) - 2.0” (5.08 cm)
With riser Ø2”	36” (91.4 cm)	1.0”(2.54 cm)	2.0” (5.08 cm)

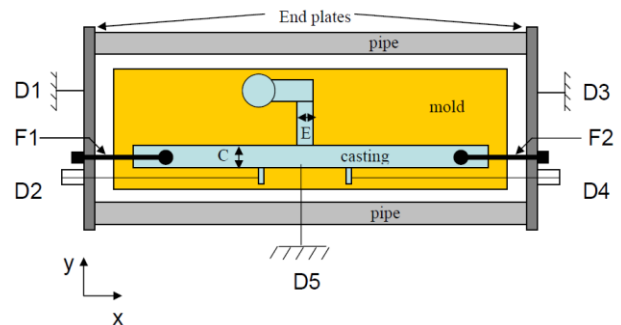


Fig. 28. The new-experimental “T” Shape casting scheme [69]

The mould was also developed by observing the distortion value occurring in the hot tearing specimen, through the addition of LVDT and Load cell in the most affected area [69]. This is because LVDT is used to measure deformation on the specimens labelled with specific symbols, such as D2, D4, and D5. It is also used in measuring plate deformations due to the freezing of specimens. Based on this study, a ~9000 lbs load cell was positioned on each of the two bolts near the sleeve inlet, to measure the forces (F1 and F2). Additionally, thermocouples were used to measure the freezing temperature, with the arms length and width values constantly utilized being 36” and 1”, respectively (Fig. 28).

Istrumen Constrained T-Shaped Casting (ICTC) apparatus,

This method was developed to analyse hot tearing, by eliminating the effect of constraints through the mould causing tensile and strain in the specimen [20,70,71]. The mould geometry was also designed to ensure that the cast metal specimen was free from contraction during solidification. Furthermore, the utilized sand mould contained sodium silicate bounded silica, to form a T-shape in the cast cavity. Both ends of the specimen were then provided with a 50 kN load cell placed on two steel bolts, to record real-time contraction pressure. As shown in Fig. 29, two thermocouples were placed at the hot spot (T-junction) of the specimen and the mould.

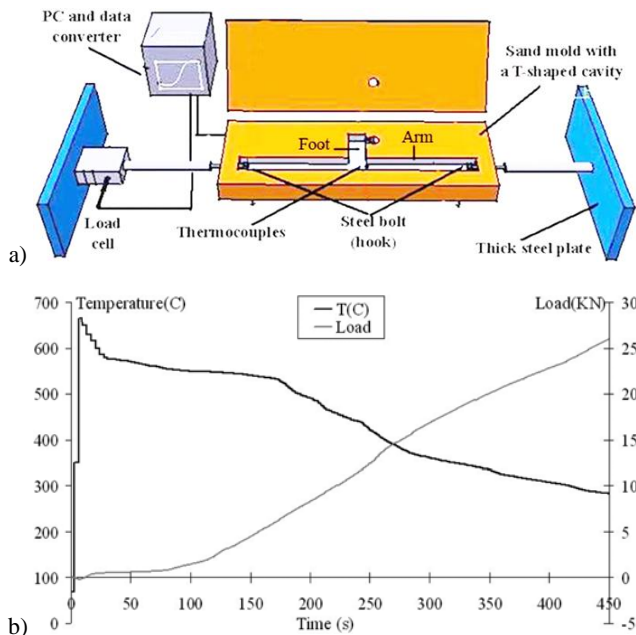


Fig. 29. (a) The schematic of ICTC apparatus for analysing hot tearing, and (b) The load and temperature-time curve [20]

Constrain Bar, Using this method, a study was conducted on hot tearing through the permanent H13 steel moulds [72]. Experimental arrangement and constrained bar schematic are shown in Fig. 30, where the sensors used for the measurement system included load cells, thermocouples, and data acquisition. The test specimen also contained two arms, each being slightly tapered to reduce friction between the mould and the cast metal during solidification. Also, the end of the right arm was pinned by steel through the graphite retainer, as the bottom of the pins were threaded and held not to move. The freezing of molten metal then began from the ends of both arms, with the left side being used to measure the load and temperature of the cast object. The threaded titanium rod was also placed on the left end and embedded in the specimen, while the other side was connected to a load cell limiting the sample contraction. This caused cracking as the titanium rods were used to reduce the thermal expansion/contraction of the rods during measurement. Additionally, two K-type thermocouples were used to measure the temperature at the riser end (T1) and specimen rod (T2).

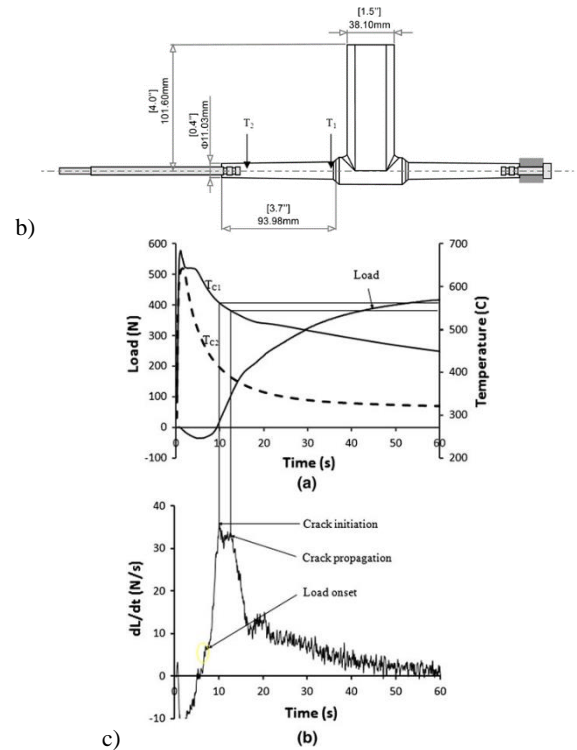
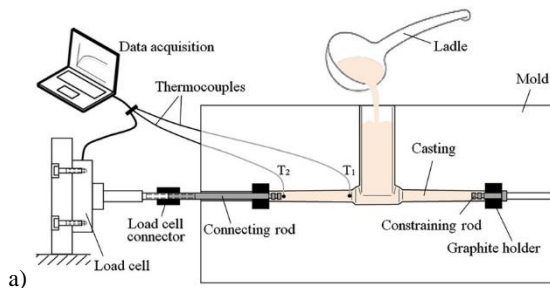
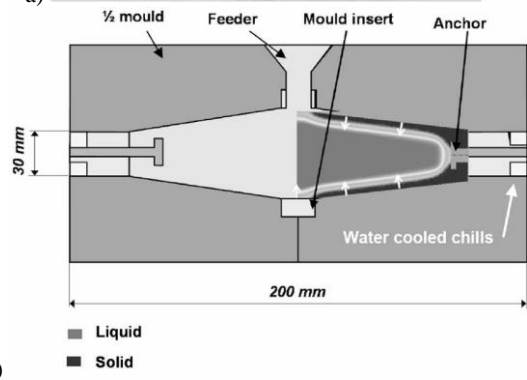
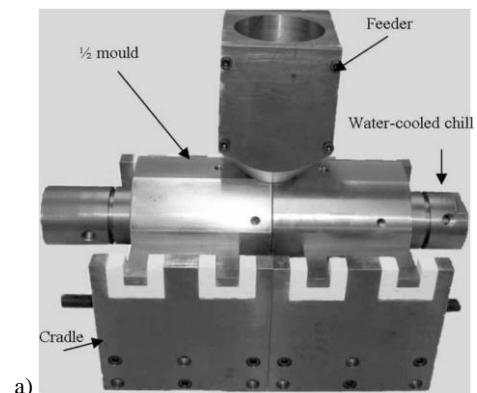


Fig. 30. (a) The experimental arrangement scheme, (b) the specimen dimensions, and (c) the temperature and load as functions of time, as well as the derivation of the load vs time curve [72]



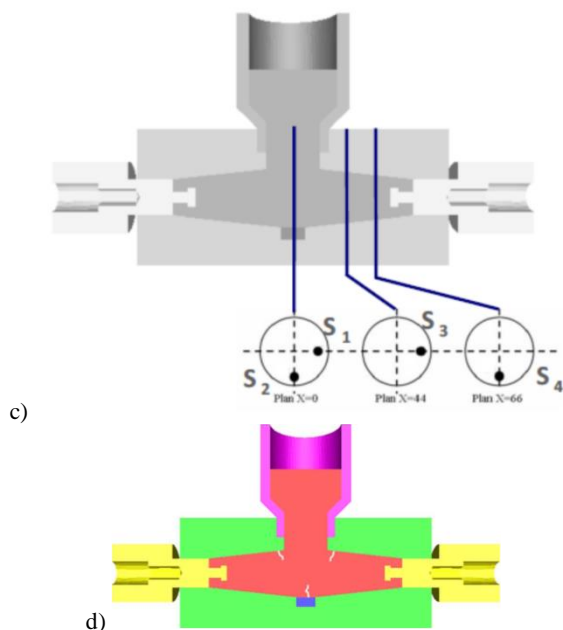


Fig. 31. (a) The experimental setup for the Crickacier hot tearing test, (b) The schematic of the Crickacier hot tearing test, (c) The location of the thermocouple placement on the specimen, and (d) The illustration of the cracking potentials (longitudinal symmetry plane) [73,74]

Crickacier Hot Tearing Test, This method was developed to analyse the process of hot tearing formation, based on the constrained solidification test. Fig. 31 shows the scheme of the Crickacier hot tearing test and the experimental setup of this study. This indicated that water-cooled chills were provided at both ends of the specimens, with freezing starting from either areas. The cast cavity for the specimen was also observed as sources of two cones, leading to a larger space and hot spot formation in the centre of the mould. Furthermore, both sample ends were provided with anchors, leading to the creation of tensile stress during solidification. The direction of the tensile stress was also perpendicular to the growth of columnar dendrites, along the specimen surface in the hot spot area. Therefore, cracks were found to be produced in the hot spot area [73,74].

CRC mould Apparatus, This was experimental on the quantitative hot tearing with CRC apparatus, which contained load cell and data acquisition system [75,76,77,63,78]. The force generated by the concentration was obtained through a load cell, as well as a data logging unit, and recording program. This indicated that hot tears generally occurred at the angle between the sprue and the horizontal rod. The mould also contained two main parts, namely a vertical sprue and a horizontal-circular rod with 148 mm length. At both ends of the sprue, the diameter of the rod was 12.5 and 10 mm (Fig. 32), where the material was tapered to reduce the friction of the metal mould specimen. At the end of the specimen, a steel rod with a length and diameter of 53 and 6 mm was inserted and connected to a load cell, respectively. Hot tearing was also analysed using the force against the time and cooling curves obtained from the load cell and thermocouple, respectively.

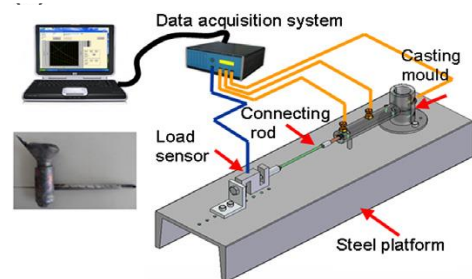


Fig. 32. (a) The experimental set up of cooling rate, (b) The CRC system schematic apparatus [79,76]

Hot tearing susceptibility was evaluated using the CSC (cracking susceptibility coefficient) with the Clyne-Davies model in Eq. (11) [11,80].

$$CSC = \frac{t_v}{t_r} = \frac{t_{0.01} - t_{0.1}}{t_{0.1} - t_{0.6}} \quad (11)$$

where t_v = the period when the stress is released into the vulnerable region, and t_r = the period when the stress is released into the relaxation region.

Rig hot tearing, This was developed by Istone [81] and modified by Davidson et al. [82], based on directly observing the hot spot area during freezing. The experimental setup allowed the simultaneous casting of two rod parts through the runner and riser within the centre of the specimen. One part of the rod was fully restrained, with the other side being an installed load cell and thermocouple connected to the data acquisition. For this process, hot spots were often formed in the centre, which was insulated with ceramic fibre insulation and a thickness of 1 mm close to the runner. A cover of 3 mm insulation was also placed over the mould, as the lid was modified by creating a window of borosilicate glass in the hot spot area. This was to directly observe the hot tear formation process on the surface of the specimen. Additionally, the fiber insulation was preheated at 200°C for 2 h, to remove moisture [14,83,84,40]. To observe hot tearing, Fig. 33a and 33b shows a plan view and camera position, respectively.

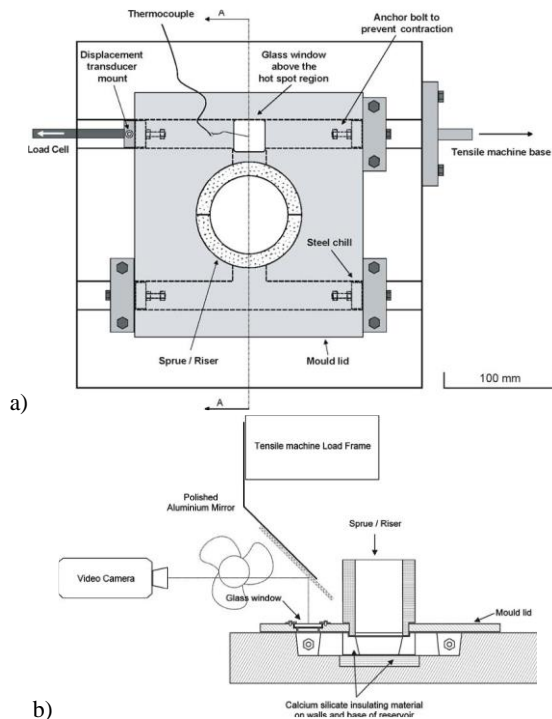


Fig. 33. (a) The plan view to observe hot tearing, and (b) The mould cut in sections A-A [82]

Thermo-Cracking-Linear Contraction Test, Hot tearing stresses were analysed using the ZQS-2000 twin Bar Tester in the Thermo-Cracking-Linear Contraction Test [85]. This indicated that specimens were created using a sand mould with a gravity system. The specimen rod test system is shown in Fig. 34, where hot spots are formed during the solidification of molten metal. During freezing, the pressure transducer recorded the tensile stress when connected to the rod of the specimen, with hot tearing resistance detected through the entire process. Ni-Cr and Ni-Si thermocouples were also placed in the hot spots, to determine the temperature characterization during freezing. The cooling curves of a Ni-Cr and Ni-Si thermocouple were then placed into a cylindrical cast chamber in a sand mould, with an outer diameter, height, and uniform wall thickness of 120, 100, and 200 mm, respectively. The thermocouple was installed in the centre of the sand mould due to the slow cooling curve, since the melt was allowed to cool in the air. During freezing, this curve was realistically assessed through the monitor screen, with five temperature characters being measured for each detected transition, based on the method of Knutine et al. [86].

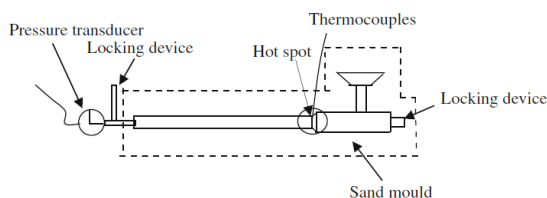


Fig. 34. The schematic of ZQS-2000 twin bar tester for Thermo-Cracking-Linear Contraction [85].

I-Beam Cracking Test, This was constructed as shown in Fig. 35 [87], where the length was 95 mm, with the insulating paper being placed in the centre of the print (19 mm wide and 1 mm thick). The last freezing process was found to also occur in the centre of the mould.

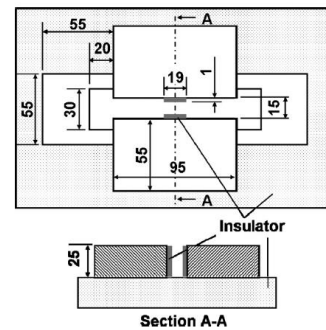


Fig. 35. The I-beam cracking casting test mould [87].

Applied Rod Casting Apparatus, The study of hot tearing in the Applied Rod Casting Apparatus (ARCA) is shown in Fig. 36a, where instrumentation equipment included load cells and transmission units, motors, data acquisition systems, and steel plates acting as retainers. The mould was also vertically divided into two parts, with the structure designed to change the dimensions of the cast space through the moving sleeve (Fig. 36b). Additionally, the casting chamber should be coated with graphite for accuracy, as the mould was then preheated with copper resistance wire wrapped at 100 mm [88].

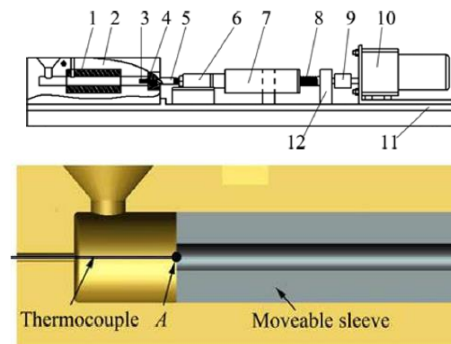


Fig. 36. The schematic of an ARCA instrument with sections, (1) Insulating material, (2) Permanent moulds, (3) Steel bolts, (4) Graphite stopper, (5) Threaded rods, (6) Load cells, (7) Binding mechanisms, (8) Trapezoidal screw, (9) Motor coupling, (10) Adjustable-speed motor, (11) Steel support plate, (12) Bearing block, and (b) movable sleeve system [88].

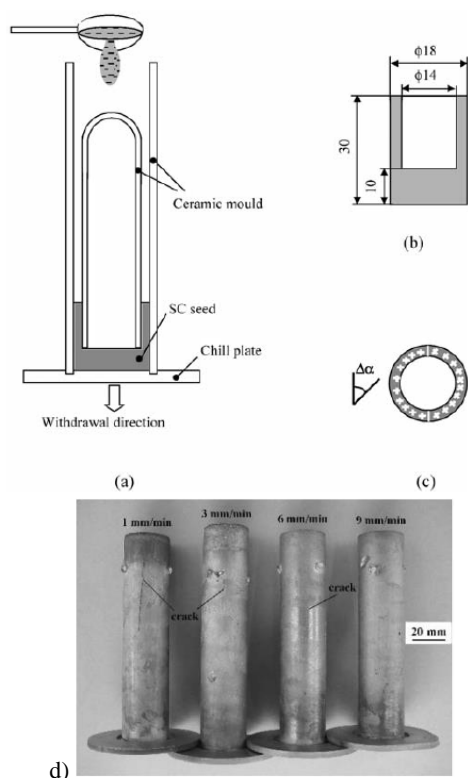


Fig. 37. The illustration of the test scheme for castability using the tube-shaped mould method, (a) an alumina mould with a single-crystal (SC) seed was used for the growth of the SC or bicrystal (BC) structure, (b) the dimensions of the SC seed, (c) the top view of the cross-section, and (d) the tube-like specimen cast BC [89,90]

Tube-Shaped Mould. Several studies have been carried out on the castability of samples having columnar grain structure, through tube-shaped mould freezing with visual observations of cast crack formations [89,90,91,92]. Fig. 37a-c shows the casting capability test schematic, as the casting with a thickness and length of 5 mm and 100-110 mm is illustrated in Fig. 37d. This indicated that the crack length obtained decreased with the increasing withdrawal rate. During solidification, the stress increased and subsequently cooled due to the difference in the thermal contraction of the mould with the alumina alloy. In addition, Fig. 38 shows the development of tube-shaped mould.

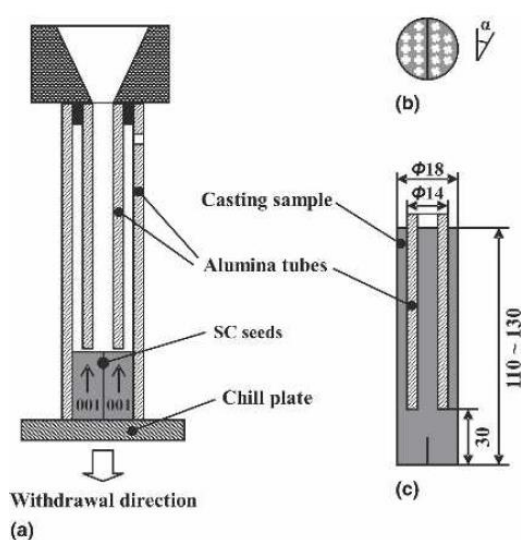


Fig. 38. The schematic illustration of the tube-shaped mould developed [91,92]

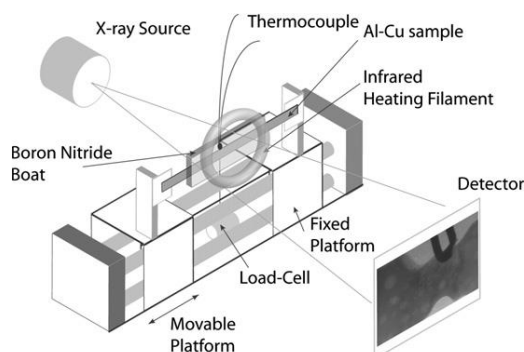


Fig. 39. The schematic of the semi-solid deformation apparatus [93]

Semi-solid deformation apparatus. The semi-solid deformation apparatus contains a tension section and an infrared furnace, as shown in Fig. 39, where axial load measurements were carried out using a 250 N Loadcell (0.1 N resolution). Crosshead movement was also performed through a two-shaft cylindrical aerostatic journal bearing, with a cable and pulley system. Moreover, semi-solid deformation was directly observed through a combination of realistic synchrotron X-ray radiography and a bespoke high-temperature tensile tester, which were produced in the solid fraction range of 0.35-0.98. During deformation, a solid fraction at a low level was observed, as medium X-ray radiography showed a significant interdendritic liquid feeding in the strain localization, before the occurrence of cracking. Local tensile deformation was also measured in the solid fractions of 0.35-0.66, with the behaviour of hot tears being consistently observed through radiography. This included limited liquid flow due to low permeability, void nucleation and coalescence, as well as final failure [93].

CRCM-Horizontal mould, According to Fig. 40, a modified-horizontal (CRCM-H) constrained rod casting mould is observed. This is a modified version of the CRC mould, whose cavity is designed to cast samples for hot tearing analysis, using six cylindrical bounded rods with 9.5 mm in diameter as well as lengths of 51 (rod A), 78.8 (rod B), 96.6 (rod C), 119.4 (rod D), 142.2 (rod E), and 165 mm (rod F), respectively. A spherical cavity and sprue at each end and base of the rod prevented free movement during shrinkage, respectively. This produced contractions (stress) on each rod when shrinking, with the spherical cavity having a diameter of 19 mm. Moreover, the cylindrical rods were separated from each other at an angle of 60°. The molten metal was also fed to the rod through a vertical sprue with a height and diameter of 60 and 29 mm, respectively [24,43,94].

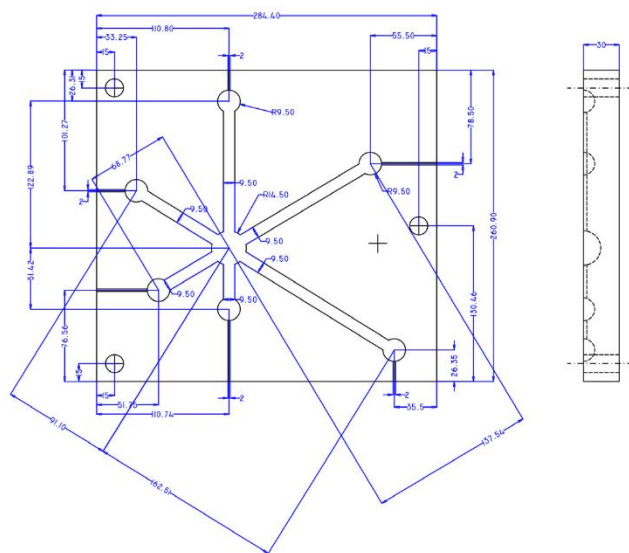


Fig. 40. The schematic of CRCM-H mould [43]

Each of the six long rods was provided with a rating of 1-6, where a RI (Rating Index) was proposed to reflect the hot tearing tendency (Fig. 40). This indicated that shorter rods were rated higher than the longer types, due to being less likely to tear. When tearing was found on the shorter rods, the severity of the problem was reflected in an alloy. The total hot tearing formed on the surface cast sample was caused by the tensile stress occurring along the rod from the sprue to the ball tips (gauge area). Furthermore, hot tearing was often found near the sprue of each rod. This indicated their rare occurrences at the end and middle of the balls and rods, respectively. The total tearing was also provided as the sum of the individual ratings for the six rods.

8. Hot Tearing Criteria

Clyne-Davies [95] and Novikov [52] criteria showed inconsistent results with casting practice, indicating no sensitivity to speed and volume position in the billet. However, the criterion was mostly used for shape casting, and was very successful in predicting hot tearing composition. According to the criteria of Feurer's [96], Katgerman [97], Magnin et al. [98], Prokhorov

[99,100], Rappaz et al. [101], and Braccini [102], the results for the casting process parameters were correctly stated, indicating that increased speed elevated the hot tearing susceptibility of the billet centre, which was consistent with the foundry practice. Meanwhile, the analytical criteria were generally not sensitive to casting speed, during the start-up phase for hot cracking, except Rappaz and Suyitno, et al. [96]. When compared to the criteria of Prokhorov, Magnin, et al., and Rappaz et al., no cracks were found under specific conditions in billet casting, to predict hot cracking. Based on the Suyitno et al., various test parameters were observed, such as casting speed and practice, lean rate, grain size, and billet position [96]. The sensitivity criterion was also a function of the selected material property value, such as Young's modulus at the mush condition, the surface tension between the liquid and solid, as well as the mush permeability. In addition, the availability of these parameters was very rare, with collection through experimental techniques found to be unreliable [103].

Feurer's Criterion, Feurer's hot tearing theory is a non-mechanical criterion focusing on feeding and shrinkage during freezing. This indicates that hot tearing occurs based on the retention of feeding material, because of the fluid flow difficulty through the mushy zone of the permeable medium, which competes with the freezing shrinkage. Two important points are also found in Feurer's criteria, namely SVG and SRG, which focuses on the maximum volumetric flow rate through the dendritic tissue, during feeding and coagulation shrinkage. Based on this criterion, $SPV < SRG$ when hot tearing is possible, indicating that the maximum volumetric rate per unit volume was obtained from Eq. (12), through the dendritic network.

$$\begin{aligned}
 SPV &= \frac{f_l^2 \lambda_2^2 P_s}{24\pi C^2 \eta L^2} \\
 P_s &= P_o + P_M - P_C \\
 P_M &= \bar{\rho} g h \\
 \bar{\rho} &= \rho_l f_l + \rho_s f_s \\
 P_C &= \frac{4\gamma_{SL}}{\lambda_2}
 \end{aligned}
 \tag{12}$$

where f_l = the volume fraction of the liquid, λ_2 = the secondary dendritic arm, P_s = the effective feeding pressure, L = the porous tissue length determined from the distance between the locations during coherence and solidus temperature, C = the tortuosity constant of the dendritic network, η = the viscosity of the liquid phase, λ_{SL} = solid interfacial energy, ρ = average density of mush state, g = the gravitational constant, h = the distance to the surface of the liquid metal, ρ_l and ρ_s = the density of the liquid and solid in the dendritic network, f_l and f_s = the solid and liquid fractions in the dendritic network, with P_o , P_M , and P_C = atmospheric, metallo static, and capillary pressure, respectively.

The volumetric freezing shrinkage was caused by the density difference between the solid and liquid phases, with the rate being solved by Eq. (13).

$$SRG = \left(\frac{\partial \ln V}{\partial t} \right) = - \frac{1}{\bar{\rho}} \frac{\partial \bar{P}}{\partial t}
 \tag{13}$$

where V = the volume of the mush freezing element with mass constant, and t = time.

Table 7.

The data used for Feurer Computing, RGD, and Braccini Criteria [96]

ρ_l	2480 kg/m ³
ρ_s	2790 kg/m ³
λ_2	10 μm
C	4.6
$\eta = \eta_L$	0.0013 Pa.s
λ_{SL}	0.84 N/m
f_s^C	0.98
E	$= f_L \cdot \lambda \mu\text{m}$
Θ	6 deg
L	60 μm
σ_{IV}	0.914 J.m ⁻²
L	300 μm
A	0

The computation data were shown in Table 7, with hot cracking susceptibility providing the liquid fraction value (f_L) for SPV = SRV, based on Feurer's criterion [96].

Clyne and Davies' Criterion, The criterion was based on Feurer's assumption at the last stage of freezing, where difficulties were observed for the free movement of liquid when strain is formed. This was not accommodated by mass and liquid feeding, indicating that the last stage was mostly prone to hot tearing. The coefficient of crack susceptibility was also obtained from the comparison of the vulnerable period (t_v) and the time available for the stress release process (t_R). Furthermore, the Hot Cracking Susceptibility coefficient (HCS) is shown in Eq. (14).

$$HCS = \frac{t_v}{t_R} = \frac{t_{0.99} - t_{0.9}}{t_{0.9} - t_{0.4}} \quad (14)$$

where $t_{0.99}$ = the time the volume of the solid fraction (f_s) equals 0.99, $t_{0.9}$ = the time f_s equals 0.9, and $t_{0.4}$ = the time f_s equals 0.4 [95,96].

Katgerman's Criterion, This is the theoretical combination of the Clyne-Davis and Feurer criteria, where the model for calculating the HCS hot cracking value is in line with Eq. (15).

$$HCS = \frac{t_{0.99} - t_{cr}}{t_{cr} - t_{coh}} \quad (15)$$

where $t_{0.99}$ = the time f_s equals 0.99, $t_{0.9}$ = the time f_s equals 0.9, t_{coh} = the time when f_s is at the point of coherence, and t_{cr} = the time feeding becomes inadequate. The time of t_{cr} is determined using the Feurer Criterion and the period when SPV = SRG [96].

Prokhorov's Criterion, Prokhorov is the formula for the mechanical criterion, where the hot cracking sensitivity is determined by the shrinkage and apparent strain rate in the mushy condition. This is related to the SRF (strain rate fraction) of the mush, as the effect of environmental shaping is calculated by the apparent strain rate. During solidification, the alloy assumably passed through a low-ductility range known as the BTR (brittle temperature range), which began from the coherence temperature to the solid calcination. In addition, the minimum fracture strain is $D_{min.}$, whose differences with the linear free shrinkage ($\Delta\epsilon_{free}$) and

apparent strain ($\Delta\epsilon_{app}$) is entirely within the brittle temperature range (BTR). The opposite of hot tearing strain ($\Delta\epsilon_{res}$) is also the minimum interval value in Eq. (16).

$$\Delta\epsilon_{res} = \min(D_{min} - \Delta\epsilon_{free} - \Delta\epsilon_{app})$$

or (16)

$$\frac{\Delta\epsilon_{res}}{BTR} = \frac{D_{min} - (\Delta\epsilon_{free} + \Delta\epsilon_{app})}{BTR}$$

since $\dot{\epsilon} = \frac{\Delta\epsilon}{BTR} \dot{T}$, where $\dot{\epsilon}$ = strain rate, and \dot{T} = the freezing curve.

$$\dot{\epsilon}_{res} = \dot{\epsilon}_{min} - \dot{\epsilon}_{free} - \dot{\epsilon}_{app} \quad (17)$$

Hot tear was then formed in solidified body when $\dot{\epsilon}_{res} \leq 0$, or

$$\dot{\epsilon}_{res} \leq \dot{\epsilon}_{free} + \dot{\epsilon}_{app} \quad (18)$$

The criteria was also used to qualitatively and quantitatively predict hot tearing practices. This indicated that Eq. (17) was qualitatively utilized in this study, regardless of the formation hot tearing, although was very sensitive to the constitutive behaviour of the mush, which was precisely unknown. Meanwhile, Eq. (18) was used for a more qualitative prediction, where the hot tearing susceptibility was obtained from the inverse strain rate of $\dot{\epsilon}_{res}^{-1}$. The principal strain rates of $\dot{\epsilon}_{free}$ and $\dot{\epsilon}_{app}$ were also determined from the FEM analysis. Calculating the reverse strain rate of $\dot{\epsilon}_{res}^{-1}$, this was set to 10000 when $\dot{\epsilon}_{res} \leq 0$ [96,100]. Labelled with PRO in [74], this criteria was expressed in Eq. (19) as follows,

$$HCC_{PRO} = \frac{Max}{BTR} (\hat{\epsilon} - \hat{\epsilon}_c) \quad (19)$$

$$\text{With } \hat{\epsilon} = D_{min} \frac{|\dot{T}|}{BTR}$$

These criteria were based on the comparison between the damaging $\hat{\epsilon}$ and acceptable strain rates in solidifying the material of $\hat{\epsilon}_c$, where D_{min} = the fracture strain in BTR, \dot{T} = the freezing rate, and BTR = the brittleness interval amplitude ($^{\circ}\text{C}$).

Novikov's Criterion, This considered hot cracking sensitivity as determined by the shrinkage mush strain, according to the FMS (fracture much strain). It also ignores the strain observed when using the Prokhorov Criterion. Moreover, the proposed "reserve plasticity" (P_r) in the freezing range was the differential-difference between the failure elongation (ϵ_{fr}) and the linear shrinkage (ϵ_{sh}). Integration was also carried out from the coherence temperature to the solidus calcination, which was known as the BTR of ΔT_{br} in Eq. (20). Subsequently, hot tearing vulnerability was provided as P_r^{-1} , where p is expressed as follows,

$$P_r = \frac{1}{\Delta T_{br}} \int_{T_{coh}}^{T_{sol}} (\epsilon_{fr} - \epsilon_{sh}) dT \quad (20)$$

where T_{coh} and T_{sol} = the coherence and solidus temperatures. This was to determine the hot cracking susceptibility to the linear shrinkage strain, with FEM in the semisolid region, where FS (fracture strain) was obtained from experimental Al-4.5 Cu [52,97].

Strain-based Criterion, This was introduced by Magnin et al., based on the experience of strain during deep solidification. It was also in line with the final solidification FS, where Hot Cracking Sensitivity (HCS) was obtained as a quotient of circular plastic strain ($\varepsilon_{\theta\theta}$). This was observed at the solidus and experimental temperatures determined from the fracture strain of ε_{fr} , as shown in Eq. (21).

$$HCS = \frac{\varepsilon_{\theta\theta}}{\varepsilon_{fr}} \quad (21)$$

This indicated that a crack was formed when the HCS was greater than one, showing that the model was used to qualitatively and quantitatively predict hot tearing. In this calculation, $\varepsilon_{\theta\theta}$ was obtained from the FEM simulation, with ε_{fr} being 0,0018 [96].

RGD Criterion, This criteria and pressure depression of Δp_{mush} were calculated using Eq. (22) as follows,

$$\Delta p = \Delta p_{sh} + \Delta p_{mec} - \rho gh \quad (22)$$

where Δp_{sh} and Δp_{mec} = the pressure drop contributing to the mush associated with freezing shrinkage and deformation, ρ = density, g = the gravitational constant, and h = the distance to the bottom of the molten metal.

The pressure drop contributing to the mush associated with the freezing shrinkage and deformation affecting the fluid flow was also calculated through Eq. (23) as follows,

$$\Delta p_{sh} + \Delta p_{mec} = \frac{180\mu\Delta T}{G\lambda_2^2} \left[v_T \beta A + \frac{(1 + \beta)B\dot{\varepsilon}\Delta T}{G} \right] \quad (23)$$

$$A = \frac{1}{\Delta T} \int_{T_{end}}^{T_{mf}} \frac{f_s^2 dT}{(1 - f_s)^2}; B = \frac{1}{\Delta T} \int_{T_{end}}^{T_{mf}} \frac{f_s^2 \cdot f_s(T)}{(1 - f_s)^3} dT; F_s(T) = \frac{1}{\Delta T} \int_{T_{end}}^T f_s dT$$

where μ = the dynamic viscosity of the liquid phase, T = the temperature, G = the thermal gradient, λ_2 = the dendritic arm, v_T = the casting speed, β = the clotting shrinkage factor, $\dot{\varepsilon}$ = the vicoplastic strain rate, f_s = the volume fraction of solid, T_{end} = the temperature at the bridging arm of the dendrite when the grains start to form, and T_{mf} = the mass feeding temperature.

To measure hot cracking susceptibility, the depression pressure of Δp was utilized, indicating that the criteria with critical predictive load preliminaries of 2 kPa caused the formation of hot tear when $\Delta p > \Delta p_c$ [96].

Criterion of Braccini et al., This showed that the stress rates for crack initiation and propagation are shown in Eq. (24),

$$\dot{\varepsilon}^c = \left(1 - \frac{e}{l}\right) \left[\frac{\lambda - a}{\lambda} \left(\frac{2}{3} \frac{P_c - P_M}{K(T, f_s)} \right) \right]^{1/m} + \frac{e}{l} \frac{2K}{(\lambda - a)^2} \frac{P_c}{\eta_L} \quad (24)$$

$$P_c = \frac{4 \cos \theta \sigma_{lv}}{e}$$

$$P_M = \bar{\rho} gh$$

$$\bar{\rho} = \rho_l f_l + \rho_s f_s$$

$$K = \frac{e^2}{32} (1 - f_s)(f_s^c - f_c)^{1.3}$$

where $\dot{\varepsilon}^c$ = the critical strain rate for hot tearing, e = the thickness of the liquid film, l = the measurement length, λ = half the grain size, a = the length of tear, P_c = cast room pressure, P_M = the metallic pressure, K = a constitutive parameter as a function of temperature T and solid fraction (f_s), m = the strain rate sensitivity, K = the permeability at *mushy zone*, μ_L = the viscosity of the liquid, h = the distance from under the liquid metal, and f_s^c = the solid fraction during the liquid network separation. In addition, the critical strain rate of $\dot{\varepsilon}^c$ was obtained from hot tearing susceptibility [96].

Effective Tearing Strain Criterion, There are many different criteria for quantifying hot tearing susceptibility, with liquid pressure drop and feeding difficulty being the parameters developed by Rapaz et al. Another concept is the critical strain and stress, where two hot tearing conditions were used in the “Two-Phase Model” when the subject of TS (tensile stress) was not considered [104], namely the liquid feeding difficulty and local thermal deformation, as well as the viscoplastic coagulation tissue dilatation. The mushy zone phenomenon and the new criteria also occurred by combining all the model phenomena, which is commonly known as the effective tearing strain.

$$\Delta \varepsilon(w_v, w_d) = \left\{ \begin{array}{l} 0 \text{ untuk } p_l(g_s = g_s^{nof}) \geq p_c \\ (w_v \cdot tr(\dot{\varepsilon}_s^p) + w_d \cdot \dot{\varepsilon}_s^{-p}) dt \text{ untuk } p_l(g_s = g_s^{nof}) < p_c \end{array} \right\} \quad (25)$$

This indicated that hot tearing occurred when $\Delta \varepsilon$ was greater than the critical value ($\Delta \varepsilon_c$). Subsequently, these criteria were rationalized as follows, (1) the strain in Eq. (25) indicated that hot tearing was formed with the availability of liquid feeding. This showed that Rapaz et al. previously identified the critical liquid pressure (p_c) quantifying the ability of feeding, to achieve the deepest part of the mushy zone [104].

Won-Oh Criterion, This focuses on the Solid Mechanics in Eq. (26), due to being the development of the YAM criteria, including the effect of strain rate [77].

$$HCC_{WYSO} = \frac{Max}{BTR} \left(\int \hat{\varepsilon}(t) dt - \hat{\varepsilon}_c \right) \quad (26)$$

with $\hat{\varepsilon} = \frac{\varphi}{(\dot{\varepsilon})^{m^*} BTR^{n^*}}$

This indicated that three parameters were deduced by the nonlinear data covering various tests on medium steel, i.e., $\varphi=0.02821$, $m^*=0.3131$, and $n^*=0.8638$. These results were observed when the strain limit criteria $\hat{\varepsilon}_c$ was a material datum.

Niyama Criterion, This criterion is a standard used in the metal casting industry, to measure the feeding formation potential based on porosity shrinkage, as shown in Eq. (27) [105].

$$\begin{aligned}
 N_y &= G/\sqrt{\dot{T}} \\
 Ny^* &= \sqrt{\frac{\Delta P_{cr} \lambda_2^2 G}{\beta \mu_1 \Delta T_f \sqrt{\dot{T}}}} \\
 \varepsilon^* &= \frac{\Delta T_f \dot{\varepsilon}}{\dot{T}} \\
 N^* &= \sqrt{I_{sh}(g_{1,cr}) + \frac{1+\beta}{\beta} \varepsilon^* I_d(g_{1,cr})}
 \end{aligned} \quad (27)$$

Besides Novikov, the stress-based criteria were also introduced by Dickhaus et al., Lahaie and Bouchard, Langlais and Gruzleski, as well as Williams and Singer [1]. Subsequently, the strain rate-based criteria were established by Stangeland, Mo, and Eskin [1]. This indicated that the modifications to the Clyne-Devis criteria were then influenced by grain size and solidification ranger (criteria based on other principles) [1]. In line with Sadayappan and Apelian criteria, calculations were also carried out on hot tear application through constrained permanent mould [106].

9. Summary

The hot tear phenomenon is a complex phenomenon that is influenced by heat flow, fluid flow, mass flow, and various other forming factors such as alloy composition, casting design, pouring temperature, mould temperature, pouring speed, mould design complexity, grain structure refinement. Hot tearing can be prevented from developing by controlling some of these casting processes. Pouring and mould temperatures, grain refinement as well as pouring speed can affect tear formation. Several studies explain that both pouring temperature and mould temperature have a large impact and can have a small impact on tear propagation. This is greatly influenced by the chemical composition of the alloy. While the design of the mould determines the formation of thermal contraction during solidification of metal alloys. The ability of the product to move freely during shrinkage greatly initiates cracking. The short length of the cast product will determine the short length of the shrinkage movement. In addition, the literature explains generally the shape of metal grains will affect the formation of hot tears. The shape of columnar and equiaxed grain morphology affects working loads due to mould constrain, thermal contraction, and shrinkage. Moreover, the prediction of hot tearing was calculated through several criteria, as various conditions were also being developed to accurately predict the formation of hot tears.

Acknowledgments

This research was funded by a grant from the Research Fund of the Ministry of Education, Culture, Research and Technology (Mendikbudristek), the Republic of Indonesia, and LPPM Universitas Syiah Kuala. Author would like thank to Dr. Viktor Malau, Dr. Priyo Tri Iswanto, and Dr. Suyitno, for discussions.

References

- [1] Li, S. & Apelian, D. (2011). Hot Tearing of aluminum alloy: a critical literature review. *International Journal of Metalcasting*. 5(1), 23-40.
- [2] Kumar, V.M. & Devi, C.N. (2014). Evaluation of mechanical characteristics for aluminum-copper metal matrix composite. *Research Journal of Engineering Sciences*. 3(3), 1-5.
- [3] Briggs, C.W. & Gezelius, R.A. (1934). Studies on solidification and contraction in steel castings II-Free and hindered contraction of cast carbon steel. *AFA Trans.* 42, 449-476.
- [4] Körber, F. & Schitzkowski, G. (1928). Determination of the contraction of cast steel. *Stahl Und Eisen*. 15, 128-135.
- [5] Verö, J. (1936). The hot-shortness of aluminum alloys. *The Metals Industry*. 48, 431-434.
- [6] Pumphrey, W.I. & Jennings, P.H. (1948). A consideration of the nature of brittleness at temperature above the solidus in castings and welds in aluminum alloys. *Journal of Institute of Metals*. 75, 235.
- [7] Pellini, W.S. (1952). Strain theory of hot tearing. *Foundry*. 80, 125-199.
- [8] Rosenberg, R.A. Flemings, M.C. & Taylor, H.F. (1960). Nonferrous binary alloys hot tearing. *AFS Transactions*. 69, 518-528.
- [9] Saveiko, V.N. (1961). Theory of hot tearing. *Russian Castings Production*. 11, 453-456.
- [10] Metz, S.A. & Flemings, M.C. (1970) A fundamental study of hot tearing. *AFS Transactions*. 78, 453-460.
- [11] Clyne, T.W. & Davies, G.J. (1975). A quantitative solidification test for casting and an evaluation of cracking in aluminium-magnesium alloys. *The British Foundryman*. 68(9), 238-238.
- [12] Campbell, J. (1991). *Castings*. Oxford: Butterworth-Heinemann.
- [13] Sigworth, G.K. (1996). Hot tearing of metals. *AFS Transactions*. 104, 1053-1062.
- [14] Davidson, C., Viano, D., Lu, L., & Stjohn, D. (2006). Observation of crack initiation during hot tearing. *International Journal of Cast Metals Research*. 19, 59-65.
- [15] Singer, K., Benek, H. (1931). Contribution to hot tears in steel castings. *Stahl and Sisen*. 51, 61-65.
- [16] Middleton, J.M. & Protheroe, H.T. (1951). The hot-tearing of steel. *Journal of the Iron and Steel Institute*. 168, 384-397.
- [17] Bichler, L., Elsayed, A., Lee, K. & Ravindran, C. (2008). Influence of mold and pouring temperatures on hot tearing susceptibility of AZ91D magnesium alloy. *International Journal of Metalcasting*. 2(1), 43-54.
- [18] Couture, A. & Edwards, J.O. (1996) The hot-tearing of copper-base casting alloys. *AFS Transactions*, 74, 709-721.
- [19] Karunakar, D.B., Rai, R.N., Patra, S. & Datta, G.L. (2009). Effects of grain refinement and residual elements on hot tearing in aluminum castings. *The International Journal of Advance Manufacturing Technology*. 45, 851-858.
- [20] Nasresfahani M.R. & Niroumand, B. (2010). Design of a new hot tearing test apparatus and modification of its operation. *Metals and Materials International*. 16(1), 35-38.
- [21] Burapa, R., Rawangwong, S., Chathong, J. & Boonchouytan, W. (2013). Effects of mold temperature and casting temperature on hot cracking in Al-4.5 wt.% Cu alloy.

- Advanced Materials Research.* 747, 623-626
doi:10.4028/www.scientific.net/AMR.747.623.
- [22] He, Y., Li, S., Sadayappan, K. & Apelian, D. (2013). Thermomechanical simulation and experimental characterisation of hot tearing during solidification of aluminium alloys. *International Journal of Cast Metals Research.* 26(2).
- [23] Huang, H., Fu, P., Wang, Y., Peng, L. & Jiang, H. (2014). Effect of pouring and mold temperatures on hot tearing susceptibility of AZ91D and Mg–3Nd–0.2Zn–Zr Mg alloys. *Transactions of Nonferrous Metals Society of China.* 24(4), 922-929.
- [24] Hasan, A. & Suyitno (2015). Effect pouring temperature on casting defect susceptibility of hot tearing in metal alloy Al-Si. *Applied Mechanics and Materials.* 758, 95-99.
- [25] Birru, A.K. & Karunakar, D.B. (2016). Effects of grain refinement and residual elements on hot tearing of A713 aluminium cast alloy. *Transactions of Nonferrous Metals Society of China.* 26, 1783-1790.
- [26] Apelian, D. (2009). *Aluminium cast alloys: enabling tools for improved performance.* NADCA.
- [27] Spittle, J.A. & Cushway, A.A. (1983). Influence of superheat and grain structure on hot-tearing susceptibilities of Al-Cu alloy castings. *Metals Technology.* 10(1), 6-13.
- [28] Limmaneevichitr, C., Saisiang, A. & Chantum, S. (2002). The role of grain refinement on hot crack susceptibility of aluminum alloy permanent mold castings. *Proceedings of the 65th World Foundry Congress.*
- [29] Sadayappan, M., Sahoo, M. & Weiss, D. (2007). Evaluation of the hot tear susceptibility of selected magnesium casting alloys in permanent molds. *AFS Transactions.* 115, 761-766.
- [30] Fasoyinu, Y., Sahoo, M. & Sikorski, S. (2008). Hot tearing of aluminum alloys 206 and 535 poured in metal mold. *Proceedings of the AFS 6th International Conference on Permanent Mold Casting of Aluminum and Magnesium.* 11-25.
- [31] Zhen, Z., Hort, N., Utke, O., Huang, Y., Petri, N. & Kainer, K.U. (2009). Investigations on hot tearing of Mg-Al binary alloys by using a new quantitative method. *Magnesium Technology.*
- [32] Pokorny, M.G., Monroe, C.A. & Beckermann, C. (2009). Prediction of deformation and hot tear formation using a viscoplastic model with damage. The minerals. *Metal and Materials Society.* 198-198.
- [33] Nabawy, A.M. Samuel, A.M., Samuel, F.H. & Doty, H.W. (2012). Influence of additions of Zr, Ti–B, Sr, and Si as well as of mold temperature on the hot-tearing susceptibility of an experimental Al–2% Cu–1% Si alloy. *Journal of Materials Science.* 47(9), 4146-4158.
- [34] Srinivasan, A., Wang, Z., Huang, Y., Beckmann, F., Kainer, K.U. & Hort, N. (2013). Hot tearing characteristics of binary Mg-Gd alloy castings. *Metallurgical and Materials Transactions A.* 44(5), 2285-2298.
- [35] Wang, Z., Huang, Y., Srinivasan, A., Liu, Z., Beckmann, F., Kainer K.U. & Hort, N. (2014). Experimental and numerical analysis of hot tearing susceptibility for Mg–Y alloys. *Journal of Materials Science.* 49, 353-362.
- [36] D’Elia, F., Ravindran, C., Sediako, D., Kainer, K.U. & N.Hort. (2014). Hot tearing mechanisms of B206 aluminum–copper alloy. *Materials & Design.* 64, 44-55.
- [37] Easton, M., StJohn, D.H. & Sweet, L. (2009). Grain refinement and hot tearing of aluminium alloys - how to optimise and minimise. *Material Science Forum.* 630, 213–221. <https://doi.org/10.4028/www.scientific.net/msf.630.213>.
- [38] Elsayed, A., Ravindran, C. & Murty, B.S. (2011). Effect of Al-Ti-B based master alloys on grain refinement and hot tearing susceptibility of AZ91E magnesium alloy. *Materials Science Forum.* 690, 351–354.
- [39] Choi, H., Cho, W., Konishi, H., Kou, S. & Li, X. (2012). Nanoparticle-induced superior hot tearing resistance of A206 alloy. *Metallurgical and Materials Transactions A,* 44(4), 1897-1907.
- [40] Sweet, L., Easton, M.A., Taylor, J.A., Grandfield, J.F., Davidson, C.J., Lu, L., Couper, M.J. & StJohn, D.H. (2012). Hot tear susceptibility of Al-Mg-Si-Fe alloys with varying iron contents. *Metallurgical and Materials Transactions A.* 44(12), 396-5407.
- [41] Suyitno, Savran, V.I., Katgerman, L. & Eskin, D.G. (2004). Effects of alloy composition and casting speed on structure formation and hot tearing during direct-chill casting of Al-Cu alloys. *Metallurgical and Materials Transactions A.* 35A, 3551–3561.
- [42] Bozorgi, S., Haberl, K., Kneissl, C., Pabel, T. & Schumacher, P. (2011). Effect of alloying elements (magnesium and copper) on hot cracking susceptibility of AlSi7MgCu-Alloys. In Tiryakioğlu, M., Campbell, J., and Crepeau, P.N. (eds.) *Shape Casting: The 4th International Symposium.* Wiley.
- [43] Malau, V., Akhyar, H., Iswanto, P.T. (2018). Modification of constrained rod casting mold for new hot tearing measurement. 63(3), 1201-1208. DOI 10.24425/123792.
- [44] Gowri, S. & Bouchard, M. (1994). Hot cracking in aluminium alloys-part 1. Literature survey. *Research Report. Université du Québec à Chicoutimi.*
- [45] Pegguleryuz, M.O., Li, X., & Aliravci, C.A. (2009). In-situ investigation of hot tearing in aluminum alloy AA1050 via acoustic emission and cooling curve analysis. *Metallurgical and Materials Transactions A.* 40(6), 1436-1456.
- [46] Purvis, A.L., Kannatey-Asibu, E. & Pehlke, R.D. (1990). Evaluation of acoustic emission from isand cast alloy 319 during solidification and formation of casting defects. *AFS Transactions.* 98, 1-7.
- [47] Purvis, A.L., Kannatey-Asibu, E. & Pehlke, R.D. (1991). Acoustic emission signal characteristics from casting defects formed during solidification of Al alloy 319. *AFS Transactions.* 102, 525-530.
- [48] Birru, A.K., Karunakar, D.B. & Mahapatra, M.M. (2012). A study on hot tearing susceptibility of Al–Cu, Al–Mg, and Al–Zn alloys. *Transactions of the Indian Institute of Metals.* 65(1), 97–105.
- [49] Singer, A.R.E. & Jennings, P.H. (1946). Hot-shortness of the aluminium-1043 silicon alloys of commercial purity. *Journal of Institute of Metals.* 72, 197-211.
- [50] Gamber, E.J. (1959). Hot cracking test for light metal casting alloys. *Trans. AFS.* 67, 237-237.

- [51] Lemieux, A., Langlais, J. & Chen, X. (2013). Reduction of hot tearing of cast semi-solid 206 alloys. *Solid State Phenomena*. 193, 101-106.
- [52] Novikov, I.I. (1966). Hot shortness of non-ferrous metals and alloys. *Moscow, Nauka*, 299. (in Russian)
- [53] Zych, J., Myszka, M., Snopkiewicz, T. (2017). Hot cracking tendency of non-ferrous alloys - a new test method. W *Nauka i Technologia 2017 – Odlewnictwo Metali Nieżelaznych*, 199-212. Kraków: Wydawnictwo Naukowe „Akapit”. (in Polish).
- [54] Oya, S., Honma, U., Fujii, T. & Othaki, M. (1984). Evaluation of hot tearing in binary Al-Si alloy castings. *Aluminium*. 60(20), 777.
- [55] Warrington, D. & McCartney, D.G. (1989). Development of a new hot-cracking test for aluminum alloys. *Cast Metals*. 2, 134.
- [56] Lin, S., Aliravci, C. & Pekguleryuz, M.O. (2007). Hot-tear susceptibility of aluminum wrought alloys and the effect of grain refining. *Metallurgical and Materials Transactions A*. 38(5), 1056-1068.
- [57] Cao, G. & Kou, S. (2006). Hot cracking of binary Mg–Al alloy castings. *Materials Science and Engineering: A*. 417 (1-2), 230-238.
- [58] Wannasin, J., Schwam, D., Yurko, J.A., Rohloff, C. & Woycik, G. (2006). Hot tearing susceptibility and fluidity of semi-solid gravity cast Al-Cu alloy. *Solid State Phenomena*. 116-117, 76-79.
- [59] Lin, S., Aliravci, C. & Pekguleryuz, M.O. (2007). Hot-tear susceptibility of aluminum wrought alloys and the effect of grain refining. *Metallurgical and Materials Transactions A*. 38(5), 1056-1068.
- [60] Guo, J. & Zhu, J.Z. (2007). Prediction of hot tearing during alloy solidification. In *the 5th Decennial International Conference on Solidification Processing*. Columbia. USA, 549-553.
- [61] Kanga, H.K., Larouche, D., Bournane, M. & Rahem, A. (2010). Hot tearing of aluminum–copper B206 alloys with iron and silicon additions. *Materials Science and Engineering: A*. 527(27-28), 7413-7423.
- [62] Cao, G., Zhang, C., Cao, H., Chang, Y.A. & Kou, S. (2010). Hot-tearing susceptibility of ternary Mg-Al-Sr alloy castings. *Metallurgical and Materials Transactions A*. 41(3), 706-716.
- [63] D’Elia, F., Ravindran, C., Sediako, D., Kainer, K.U. & Hort, N. (2014). Hot tearing mechanisms of B206 aluminum–copper alloy. *Materials & Design*. 64, 44-55, <https://doi.org/10.1016/j.matdes.2014.07.024>.
- [64] Bichler, L. & Ravindran, C. (2010). New developments in assessing hot tearing in magnesium alloy castings. *Materials and Design*. 31, 17-23.
- [65] Li, S. (2010). Hot Tearing in cast aluminum alloys: measures and effects of process variables. *Worcester Polytechnic Institute*. 24-24.
- [66] Myszka, M., Zych, J. & Snopkiewicz, T. (2018). Hot cracking tendency of foundry alloys – an innovative testing method. *Prace Instytutu Odlewnictwa Transactions of the Foundry Research Institute*. 58(4), 235-249. DOI: 10.7356/ioc.2018.19.
- [67] Monroe, C. & Beckermann, C. (2004). Development of a hot tear indicator for steel castings. In *The 58th SFSA Technical and Operating Conference*. Chicago, America, 1-13.
- [68] Monroe, C. & Beckermann, C. (2005). Development of a hot tear indicator for steel castings. *Materials Science and Engineering A*. 413-414(3), 30-36.
- [69] Monroe, C.A., Beckermann, C. & Klinkhammer, J. (2009). Simulation of deformation and hot tear formation using a visco-plastic model with damage, in book Cockcroft, S.L. & Maijer, D.M., eds. modeling of casting, Welding, and Advanced Solidification Processes-XII. *TSM (The Minerals, Metals & Materials Society)*. 313-320.
- [70] Nasresfahani, M.R. & Niroumand, B. (2014). A new criterion for prediction of hot tearing susceptibility of cast alloys. *Metallurgical and Materials Transactions A*. 45(9), 3699-3702.
- [71] Nasresfahani, M.R. & Rajabloo, M.J. (2014). Research on the effect of pouring temperature on hot-tear susceptibility of A206 alloy by simulation. *Metallurgical and Materials Transactions B*. 45(5), 1827-1833.
- [72] Li, S., Sadayappan, K. & Apelian, D. (2013). Role of grain refinement in the hot tearing of cast Al-Cu alloy. *Metallurgical and Materials Transactions B*. 44(3), 614-623.
- [73] Olivier, C., Yvan, C. & Michel, B. (2008). Hot tearing in steels during solidification: experimental characterization and thermomechanical modeling. *Journal of Engineering Materials and Technology*. 130(2), 021018.
- [74] Bellet, M., Cerri, O., Bobadilla, M. & Chastel, Y. (2009). Modeling hot tearing during solidification of steels: assessment and improvement of macroscopic criteria through the analysis of two experimental tests. *Metallurgical and Materials Transactions A*. 40(11), 2705-2717.
- [75] Srinivasan, A., Wang, Z., Huang, Y., Beckmann, F., Kainer, K.U. & Hort, N. (2013). Hot tearing characteristics of binary Mg-Gd alloy castings. *Metallurgical and Materials Transactions A*. 44(5), 2285-2298.
- [76] Wang, Z., Huang, Y., Srinivasan, A., Liu, Z., Beckmann, F., Kainer, K.U. & Hort, N. (2013). Hot tearing susceptibility of binary Mg–Y alloy castings. *Materials and Design*. 47, 90-100.
- [77] Srinivasan, A., Wang, Z., Huang, Y., Beckmann, F., Kainer, K.U. & Hort, N. (2013) Hot tearing characteristics of binary Mg-Gd alloy castings. *Metallurgical and Materials Transactions A*. 44(5), 2285-2298.
- [78] Liu, Z., Zhang, S., Mao, P. & Wang, F. (2014). Effects of Y on hot tearing susceptibility of Mg–Zn–Y–Zr alloys. *Transactions of Nonferrous Metals Society of China*. 24(4), 907-914.
- [79] Akhyar, H. & Husaini (2016). Study on cooling curve behavior during solidification and investigation of impact strength and hardness of recycled Al–Zn aluminum alloy. *International Journal of Metalcasting*. 10(4), 452-456. <https://doi.org/10.1007/s40962-016-0024-8>.
- [80] Clyne, B. & Davies, G.J. (1981). The influence of composition on solidification cracking susceptibility in binary alloy systems. *J. Brit Foundryman*. 74, 65-73.
- [81] Instone, S. (1999). The effect of alloy composition and microstructure on the hot cracking of vertical direct chill cast aluminium alloy billet. *University of Queensland*.
- [82] Davidson, C., Viano, D., Lu, L., D.H.S. (2005). Shape Casting, *7th International Symposium Celebrating Prof. John Campbell's 80th Birthday*.

- [83] Mitchell, J.B. Cockcroft, S.L., Viano, D., Davidson, C. & StJohn, D. (2007). Determination of strain during hot tearing by image correlation. *Metallurgical and Materials Transactions A*. 38(10), 2503-2512.
- [84] Easton, M.A., Wang, H., Grandfield, J., Davidson, C.J., StJohn, D.H., Sweet, L.D. & Couper, M.J. (2012). Observation and prediction of the hot tear susceptibility of ternary Al-Si-Mg alloys. *Metallurgical and Materials Transactions A*. 43(9), 3227-3238.
- [85] Li, M., Wang, H., Wei, Z. & Zhu, Z. (2010). The effect of Y on the hot-tearing resistance of Al-5 wt.% Cu based alloy. *Materials and Design*. 31(5), 2483-2487. <https://doi.org/10.1016/j.matdes.2009.11.044>.
- [86] Knuutinen A., Nogita K., McDonald S.D. & Dahle A.K. (2001) Modification of Al-Si alloys with Ba, Ca, Y and Yb. *Journal of Light Metals*. 229-240.
- [87] Murashima, I., Asada, J. & Yoshida, M., (2008). Effect of grain refiner and grain size on the susceptibility of Al - Mg die casting alloy to cracking during solidification. *Journal of Materials Processing Technology*. 209, 210-219.
- [88] Xu, R., Zheng, H., Luo, J., Ding, S., Zhang, S. & Tian, X. (2014). Role of tensile forces in hot tearing formation of cast Al-Si alloy. *Transactions of Nonferrous Metals Society of China*. 24(7), 2203-2207.
- [89] Zhang, J. & Singer, R.F. (2004). Effect of grain-boundary characteristics on castability of nickel-base superalloys. *Metallurgical and Materials Transactions A*. 35, 939-946.
- [90] Zhou, Y., Volek, A. & Singer, R.F. (2005). Influence of solidification conditions on the castability of nickel-base superalloy IN792. *Metallurgical and Materials Transactions A*. 36, 651-656.
- [91] Zhou, Y., Volek, A. & Singer, R.F. (2006). Effect of grain boundary characteristics on hot tearing in directional solidification of superalloys. *Journal of Materials Research*. 21(09), 2361-2370.
- [92] Zhou, Y. & Volek, A. (2008). Effect of carbon additions on hot tearing of a second generation nickel-base superalloy. *Materials Science and Engineering: A*. 479(1-2), 324-332.
- [93] Phillion, A.B., Hamilton, R.W., Fuloria, D., Leung, A.C.L., Rockett, P., Connolley, T. & Lee, P.D. (2011). In situ X-ray observation of semi-solid deformation and failure in Al-Cu alloys. *Acta Materialia*. 59, 1436-1444.
- [94] Akhyar, H., Malau, V., Suyitno & Iswanto, P.T. (2017). Hot tearing susceptibility of aluminum alloys using CRCM-Horizontal mold. *Results in Physics*. 7, 1030-1039. <https://doi.org/10.1016/j.rinp.2017.02.041>.
- [95] Clyne, G.J. & Davies, T.W. (1979). *Solidification and Casting of Metals*. London: Metals Society. 275-278.
- [96] Suyitno, Kool, W. H., Katgerman, L., (2005). Hot Tearing Criteria Evaluation for Direct-Chill Casting of an Al-4.5 Pct Cu Alloy. *Metallurgical and Materials Transactions A*. 36A, 1537-1546.
- [97] Katgerman, L. (1982). A mathematical model for hot cracking of aluminum alloys during D.C. casting. *JOM Journal of the Minerals Metals & Materials Society*. 34, 46-49. <https://doi.org/10.1007/BF03339110>.
- [98] Magnin, B., Maenner, L., Katgerman, L. & Engler, S. (1996). Ductility and theology of an Al-4.5%Cu alloy from room temperature to coherency temperature. *Mater Science Forum*. 1209, 217-222.
- [99] Eskin, D.G., Suyitno & Katgerman, L. (2004). Mechanical properties in the semi-solid state and hot tearing of aluminum alloys. *Progress in Materials Science*. 49, 629-711.
- [100] Prokhorov, N.N. (1962). Resistance to hot tearing of cast metals during solidification. *Russian Castings Production*. 2, 172-175.
- [101] Rappaz, M., Drezet, J.M. & Gremaud, M. (1999). A new hot-tearing criterion. *Metallurgical and Materials Transactions A*. 30A, 449-455.
- [102] Braccini, M., Martin, C. L., Suéry, M. & Bréchet, Y. (2000). Modeling of casting. *Welding and Advanced Solidification Processes IX*. 18-24.
- [103] Eskin, D.G. & Katgerman, L. (2007). A quest for a new hot tearing criterion. *Metallurgical and Materials Transactions A*. 38A, 1511- 1519, DOI: 10.1007/s11661-007-9169-7.
- [104] Hamdi, M.M., Mo, A. & Fjær, H.G. (2006). TearSim : A two-phase model addressing hot tearing formation during aluminum direct chill casting. *Metallurgical and Materials Transactions A*. 37, 3069-3083.
- [105] Monroe, C. & Beckermann, C. (2014). Prediction of hot tearing using a dimensionless niyama criterion. *The Journal of The Minerals*. 66(8), 1439-1445.
- [106] Aguiar, A.M. (2020). Hot tearing susceptibility of single-phase Al-3.8 wt%Zn-1 wt%Mg alloy using the constrained rod solidification experiment: influence of 1.2 wt%Fe addition and grain refinement. *Thesis, McMaster University*. Hamilton, Ontario.